Preprints.org

Review

Not peer-reviewed version

Enzyme-Based Single Solid-State Nanochannels Biosensors

Luis Miguel Hernández Parra , Omar Azzaroni , Waldemar Alejandro Marmisolle *

Posted Date: 2 July 2025

doi: 10.20944/preprints202507.0128.v1

Keywords: solid-state nanochannels; biosensor; enzyme; iontronics

Preprints.org is a free multidisciplinary platform providing preprint service that is dedicated to making early versions of research outputs permanently available and citable. Preprints posted at Preprints.org appear in Web of Science, Crossref, Google Scholar, Scilit, Europe PMC.

Copyright: This open access article is published under a Creative Commons CC BY 4.0 license, which permit the free download, distribution, and reuse, provided that the author and preprint are cited in any reuse.

Preprints.org (www.preprints.org) | NOT PEER-REVIEWED | Posted: 2 July 2025 doi:10.20944/preprints202507.0128.v1

Disclaimer/Publisher's Note: The statements, opinions, and data contained in all publications are solely those of the individual author(s) and contributor(s) and not of MDPI and/or the editor(s). MDPI and/or the editor(s) disclaim responsibility for any injury to people or property resulting from any ideas, methods, instructions, or products referred to in the content.

Review

Enzyme-Based Single Solid-State Nanochannels Biosensors

L. Miguel Hernández Parra, Omar Azzaroni and Waldemar Marmisollé *

Instituto de Investigaciones Fisicoquímicas Teóricas y Aplicadas (INIFTA), Departamento de Química, Facultad de Ciencias Exactas, Universidad Nacional de La Plata (UNLP), CONICET, Boulevard 113 y 64, 1900 La Plata, Argentina

* Correspondence: wmarmi@inifta.unlp.edu.ar

Abstract

Sensing technologies play a critical role in healthcare, not only for diagnosis and treatment but especially for prevention and early intervention. Recent advances in biology, medicine, and materials science have expanded the landscape of measurable biological markers and enabled the development of highly sensitive and multifunctional sensing platforms. Among the most prominent strategies in biosensing are those that take inspiration from nature, particularly through the integration of biological components such as enzymes. This review focuses on the intersection between enzymatic catalysis and solid-state single nanochannel (SSN) technologies as a promising approach for the development of advanced biosensing devices. We provide an overview of the historical background, current state of the art, and major achievements in enzyme-based biosensors and artificial nanochannel platforms, highlighting their synergistic potential. Particular attention is given to the challenges associated with enzyme integration into artificial environments, including stability and functionality retention, and the strategies employed to overcome them. Finally, we discuss the prospects and limitations of combining enzymes with SSNs, aiming to inspire future research in this emerging and multidisciplinary field.

Keywords: solid-state nanochannels; biosensor; enzyme; iontronics

1. Introduction

The solution is meaningless if the problem is invisible; treatments intended to improve health may become a serious danger without proper diagnosis. These considerations are particularly relevant when it is already too late to prevent a health problem. However, the real importance of sensing technologies in the medical and health fields lies in their ability to assess potential hazards and enable preventive measures to be taken. Great advances in human genome sequencing[1], cellular metabolism, immunology[2], proteomics[3], toxicology[4], pharmacology, neuroscience[5], and human microbiology[6], have enabled the identification of numerous new measurable targets that can be objectively monitored and evaluated as indicators of biological system functionality, pathogenic conditions, or pharmacological responses to therapeutic treatments. In this context, the necessity for high-performance measurement devices is imperative. Fortunately, existing sensing techniques are continuously improving, and new ones are in constant development to meet the growing demand. These advancements enable continuous monitoring, prevention, early diagnosis, and appropriate treatments. All of this is supported by intensive research into new materials and platforms with highly adaptable and multifunctional physicochemical properties, powerful design tools involving AI assistance, and high precision versatile fabrication techniques[7,8].

Despite all the breakthroughs and successful developments in sensing methodologies with platforms and devices achieving very high sensitivity and sub micromolar detection limits, there will

© 2025 by the author(s). Distributed under a Creative Commons CC BY license.

Preprints.org (www.preprints.org) | NOT PEER-REVIEWED | Posted: 2 July 2025 doi:10.20944/preprints202507.0128.v1

always be limitations or challenges to face in this field. The intrinsic complexity of biological systems and samples represents a primary concern. Specificity, complex matrix operation, miniaturization, in vivo detection capability, wearability, accessibility, and ease of operation are essential features of sensors currently being developed[9]. These attributes facilitate the efficient integration of sensors into diverse applications and ensure their usability by a wide range of users without requiring specialized expertise. This progress has enabled the use of common smart technology devices to digitize, process, store and transmit healthcare data in real time[10]. Historically, mankind has found in nature the greatest support to its unstoppable evolution, and living systems appear to be an inexhaustible source of inspiration. The field of sensing for healthcare and clinical purposes is no exception. The ability to study biochemical mechanisms in living organisms has not only enhanced our understanding of complex metabolic pathways but also enabled the isolation, modification, design, and production of functional biochemical structures that can be integrated into abiotic systems to develop powerful biosensing tools for specific analytical purposes[11–15].

In the context of this work, the focus will be on two functional biochemical structures that are of paramount importance. Firstly, enzymes, which have a long and fascinating history and are foundational to modern biochemistry[16–18]. Enzymes have been highly relevant in biomarker sensing not only because of their direct implications for human life but also for their ability to function without the need for a living organism, thus forming the basis for the extensive field of biosensing. After the publication of the iconic work “Electrode systems for continuous monitoring in cardiovascular surgery” in 1962 by the man now known as the “father of biosensors” Prof. Dr. L.C. Clark Jr., and his colleague C. Lyons[19], and the subsequent development of the well-known “enzyme electrode” in 1967 by S.J. Updike and G.P. Hicks[20], the scientific community realized the enormous potential of enzymes as analytical tools, highlighting their great versatility and specificity. Today, more than half a century later, enzymes continue to be a key part of advanced biosensing technologies. Their high performance in both sensing and industrial applications, along with the development of new methodologies for enzyme production, preservation, and manipulation, ensures that these efficient biological catalysts remain at the forefront of biosensing technology[21,22].

On the other hand, the study of structural properties of protein channels in biological membranes has led to an understanding of their complex transport mechanisms and facilitated the construction of versatile platforms with numerous applications in the analytical field. The last decade of the past century could be described as “The boom period of protein channel research”. The remarkable work by Prof. Dr. Roderick MacKinnon and Prof. Dr. Peter Agre (Nobel laureates in Chemistry in 2003) on protein channels in biological membranes revealed the implications of shape, size, and surface physicochemical properties on the regulation of matter transport through them[23,24]. Consequently, this understanding opened the possibility of designing and constructing abiotic structures with similar characteristics, serving countless purposes. This advancement carried the research field to a new stage at which mimicking cellular processes became the main interest, leading to the development of amphiphilic systems as the first approach, because most biochemical reactions take place inside cells or at lipid interfaces[25]. However, sooner rather than later, researchers realized that these synthetic structures are potentially useful for developing other platforms not necessarily related to functions found in living systems. Then, quickly the materials to build channels changed from being amphiphilic molecules, crown ethers, oligomers or peptides[26,27], to being structures more often completely composed of thermoplastic polymers such as PET and PC[28]. Those last have the advantage of disregarding the complexity of protein channels while retaining the desirable functional features [27]. Besides, in addition to their increased physical resistance and tolerance to different chemical environments, polymeric membrane-supported channels have the advantage of being able to be designed and constructed in a wider range of different sizes and shapes to modulate transport as required[29,30]. Figure 1 shows the timeline of the nanochannels technology.

© 2025 by the author(s). Distributed under a Creative Commons CC BY license.

Preprints.org (www.preprints.org) | NOT PEER-REVIEWED | Posted: 2 July 2025 doi:10.20944/preprints202507.0128.v1

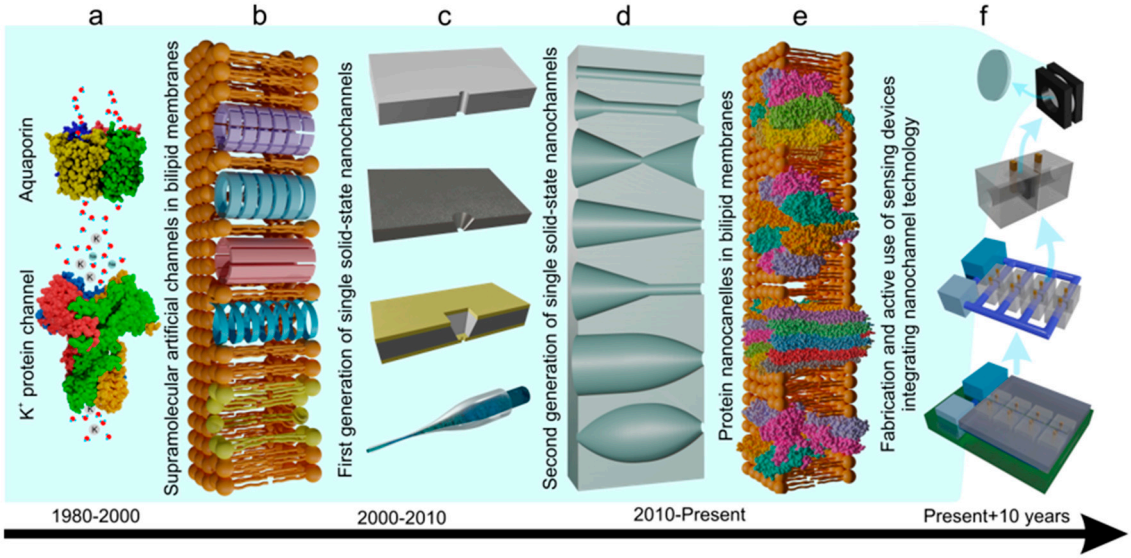

Figure 1. Timeline of nanochannel technology progress since the first studies on biological channels to the future development of sensing devices incorporating single solid state nanochannels with designed functionalities. a) Aquaporin PBD id 7W7R[31], The potassium 2.1 channel PBD id 8QQL[32]. b) supramolecular nanopores in bilipid membranes, c) The first SSNs in polymeric, silicon and glass platforms[26,27,33]. d) Ion-track etching SSN supported in polymeric membranes[34]. e) Biological protein nanochannels in bilipid membranes PDB id 2OAU[35], PDB id 3ANZ[36], PBD id 4TSY[37], PBD id 6MRU [26,35,38,39], f) Device concept integrating nanochannel membrane technology.

Enzymes are highly specialized molecular machines that perform distinct functions within living systems, exhibiting optimal performance in healthy individuals with adequate biochemical conditions. However, complications arise when they are extracted from their natural environment and placed in different systems with the expectation of achieving similar functionality. Factors such as denaturation, pH, temperature, ionic concentration, lack of cofactors and coenzymes, presence of inhibitors, active site blocking, and accumulation of reaction end products significantly hinder enzyme activity in artificial environments[40]. Consequently, enzyme supports and carriers have been extensively studied to develop immobilization platforms that preserve their maximum functional performance [22,41,42]. In this context, the integration of enzymes into single solid-state nanochannels (SSNs) has emerged as a sophisticated strategy to harness the benefits of both systems, developing functional devices with potential applications as biosensing tools [43,44]. Although this is a relatively young field where many questions remain to be answered, work to date has revealed impressive achievements and significant challenges. Highlighting these advances and addressing the obstacles is the main motivation for this review. It aims to explore the exciting prospects for the future of the field, while reviewing the remarkable work that laid the foundations for this area of research. Multichannel biosensors systems in membranes or porous materials, and single nanochannel platforms involving other biological recognition elements than enzymes are not in the scope of this review, and the reader is referred to complete recompilations of nanochannel works [43–48].

2. Physicochemical Aspects of Single Nanochannel System

2.1. Single Nanochannel Fabrication: Materials and Methods

Constructing single nanochannels for sensing applications presents a greater challenge than producing multichannel arrays, as controlling channel density in nanoscale environments demands advanced technological equipment. The methodologies currently employed for this purpose enable the fabrication of single nanopores with varying sizes, shapes, physicochemical properties, and

© 2025 by the author(s). Distributed under a Creative Commons CC BY license.

Preprints.org (www.preprints.org) | NOT PEER-REVIEWED | Posted: 2 July 2025 doi:10.20944/preprints202507.0128.v1

support materials, by controlling processing conditions and precursor materials accordingly. Table 1 summarizes some of the most frequently used techniques to obtain 1D single nanochannels, along with their relevant properties. Additionally, methodologies for nanopipette fabrication (e.g., bench-top method, laser pulling, and thermal pulling) are included. While nanopipettes share several functional properties with SSNs such as robustness, a wide range of functionalization possibilities, asymmetric ion transport, and current rectification. Technically, they are classified as a distinct group of nanopores[49]. Unlike SSNs, nanopipettes lack geometrical versatility, flexibility, and ease of integration into devices due to their extended length. Although enzymes can also be immobilized at the tip of nanopipettes for sensing applications, these systems will not be covered in this work. Instead, readers are referred to comprehensive and up-to-date reviews on the topic [49–54]. While various fabrication approaches will be mentioned below, special attention will be given to the description of methodologies used to fabricate individual SSNs reported as support for enzyme integration in sensing applications.

Table 1. Single nanochannel fabrication methods.

Technology	Materials	*Diameter (nm)	Shape	Reference
EBL + RIE	Si_3N_4	Around 20	Rectangular	[55]
RIE/ FIB + IBS	Si_3N_4	1,8-100	Cylindrical-bowl shaped cavity	[56]
FIB + IBS	Si_3N_4/Si	>1	Cylindrical-bowl shaped cavity	[57]
FIB	Au/Si_3N_4/Au; PFA/Si_3N_4/PFA	20-140	Conically narrowing	[58]
EE-PEO	PDMS	>100	Cylindrical	[59]
Bench-Top	Glass based	> 86	Conical	[60]
Bench-Top/Laser pulling	Glass based	> 40	hourglass	[61]
Thermal pulling	Glass based borosilicate	Around 30	Surficial (rectangular and conical)	[62]
EB + Dry etching + FIB	Silica glass substrate	58-655	Conical-Trumpet shaped	[63]
Ion track + Dry Plasma etching	PC	10-1000 variable	Etching dependent	[64]
Ion Track + UV exposure + Chemical etching	PET, PC, PP, PVDF, PI	5-300 variable		[65]
	PET	50-600 variable		[66]
Ion Track + UV exposure + Chemical/Electrochemical etching	PC	> 2 nm variable		[67]
Ion Track + Chemical/Electrochemical etching	PET, PC, PI, PVDF			[30]
Ion Track + Chemical Etching	PET, PC, PI, PVDF, PP			[68]

© 2025 by the author(s). Distributed under a Creative Commons CC BY license.

Preprints.org (www.preprints.org) | NOT PEER-REVIEWED | Posted: 2 July 2025 doi:10.20944/preprints202507.0128.v1

	PET, PC, PI, PVDF, SiO_2, Mica			[69]
	PET, PC, PI, PVDF, PP, CR39			[70]
	PET			[71]
	PET, PC	> 100 variable		[72]
	PI	10-1000 variable		[73]
	SiN	>100		[74]

Note 1. Electron beam (EB), Electron beam lithography (EBL), Reactive ion etching (RIE), Focused ion beam (FIB), Ion beam sculping (IBS), Embedding Electrospun Polyethylene Oxide Nanofibers (EE-PEO), Polyethylene terephthalate (PET), Polycarbonate (PC), polypropylene (PP), polyvinylidene fluoride (PVDF), polyimide (PI), Silicon nitride (Si_3N_4), Perfluoroalkyl passivation (PFA), polydimethylsiloxane (PDMS). *(The diameter indicated refers to the size reached by the tip or base in asymmetric channels or the average diameter of symmetric channels; some of these technologies can be used to produce single nanochannels above the μm scale.)

2.1.1. Ion-Track Chemical Etching

The ion track etching method is one of the most versatile technologies for producing 1D pores or channels in substrates made of various materials, commonly employed in sensing applications [30,44,45,75]. It is based on the highly accelerated ion irradiation of thin membranes. However, early research in this technology had a different focus. During the 1950s, the optimism surrounding the implementation of nuclear energy and the burgeoning arms race fueled extensive research into nuclear science [76,77]. This surge in interest also influenced many other scientific fields. Naturally, the need for particle detection systems with enhanced performance compared to cloud chambers and nuclear emulsions became imperative—not only to detect particle emissions but also to identify them, enabling a deeper understanding of particle behavior. Consequently, materials susceptible to irradiation damage were employed as detector screens to record the passage of charged particles generated by nuclear fission processes. When a charged particle impacts most insulating solids, it undergoes a deceleration or braking process, transferring its kinetic energy to the target material [78,79]. Depending on the initial energy of the particle and the nature of the target, the linear momentum transfer during the collision can either deflect the particle, altering its trajectory, or allow it to pass through the material in a straight line[69]. In both cases, the insulating nature of the bulk material leads to the ejection of excited electrons from their original positions, creating an "electronic collision cascade" that dissipates energy and generates "atomic collision cascades" through ion repulsion of the newly formed cations[79]. As a result, a typically permanent zone of ionization defects forms along the path of the projectile particle, known as "the track" (Figure 2a)[80].

Almost every latent track in a solid can be transformed into a pore or channel, with the key being the selection of optimal conditions to achieve the preferential dissolution of the "damaged" material[81]. This procedure was first demonstrated by Dr. Young in his 1958 work, "Etching of Radiation Damage in LiF." Using a solution of FeF_3 in CH_3COOH and HF, he made ion tracks generated by particles from U_3O_8 in a LiF crystal visible through electron micrographs, however there is some of controversy about his work[82]. Four years later, Price and Walker presented electron microscope images of etched charged-particle tracks in various materials, and their findings are also considered the first description of chemical etching[83]. These ground-breaking studies not only expanded the possibilities in particle detection but also laid the foundation for the ion track-etching method, which remains widely used today to fabricate pores and nanochannels [44,45,48,84]. Enlarging ion tracks through chemical etching offers several advantages. This method is effective in revealing tracks created by ions across a wide energy range, including low-energy ions such as those from solar wind. Under optimal conditions, ion tracks can be widened to the point of being visible under an optical microscope while still preserving critical information about the irradiating ion [78].

© 2025 by the author(s). Distributed under a Creative Commons CC BY license.

Preprints.org (www.preprints.org) | NOT PEER-REVIEWED | Posted: 2 July 2025 doi:10.20944/preprints202507.0128.v1

Beyond its simplicity, this technology is highly versatile. By employing asymmetric chemical etching, incorporating additives, or precisely controlling time and temperature, it is possible to create nanopores with various sizes, shapes, and profiles [30,85–87].

Surfactant assisted etching is the most used methodology to shaping channels employed in enzyme biosensors development (Table 2). As PET polymer foils are the main substrate to support the pores, concentrated NaOH solutions are used to preferentially dissolution of the damage material by basic hydrolysis[88–92]. In this medium, surfactants act as a decelerator of the etch rate, slowing down the chemical degradation in specific regions of the bulk material leading to asymmetric enlargement profiles. Most of the understanding of the protection effect generated by surfactant molecules during etching process is due to the extensive work by Apel and coworkers [66,72,93,94]. As it was mentioned before, the difference between etch rate of the track core and the bulk material mainly determines the channel shape, the mechanism behind considers that surfactant molecules adsorb on the polymer surface altering its susceptibility to chemical attack, at the same time, the protective layer formation depends on the available amount of surfactant species in a determinate zone that is significantly regulated by the restricted diffusion in nanometric spaces due to their size (surfactant layer thickness 2-4 nm)[72]. Figure 2 shows a schematic representation of the process to obtain a bullet-shaped nanochannel in a PET foil. When the etching solution is in contact with the foil surface, a quasi-solid layer of surfactant molecules is formed on the tip side (the smallest opening) and the etchant molecules have to diffuse through it to begin the material degradation, whereas at the base, the degradation rate depends only on the free diffusion of OH- and the degraded material. At the moment when the tip diameter is big enough to surfactant penetration, molecules get inside and cover the newly formed wall hindering the further diffusion of surfactant due to the comparable size of the pore with the protective layer, however, OH^- diffusion is not hindered. For that reason, the pore growing rate inside is higher and leads to the formation of a parabolic growing profile (Figure2b). If the process continues, the entrance hole will eventually become large enough to allow the surfactant to pass through and coat the inner walls reducing the inner radial etching rate, ensuring that the channel profile remains consistent as radial growth progresses (Figure 2c). On the other hand, the axial enlargement rate remains higher along the track core axis. This occurs because, in this region of "narrow growth front" the diameter is consistently smaller than the size of the surfactant molecules, preventing the formation of a protective layer. In the final stage, once the channel is fully developed along the axis, only radial enlargement occurs (Figure 2d).

© 2025 by the author(s). Distributed under a Creative Commons CC BY license.

Preprints.org (www.preprints.org) | NOT PEER-REVIEWED | Posted: 2 July 2025 doi:10.20944/preprints202507.0128.v1

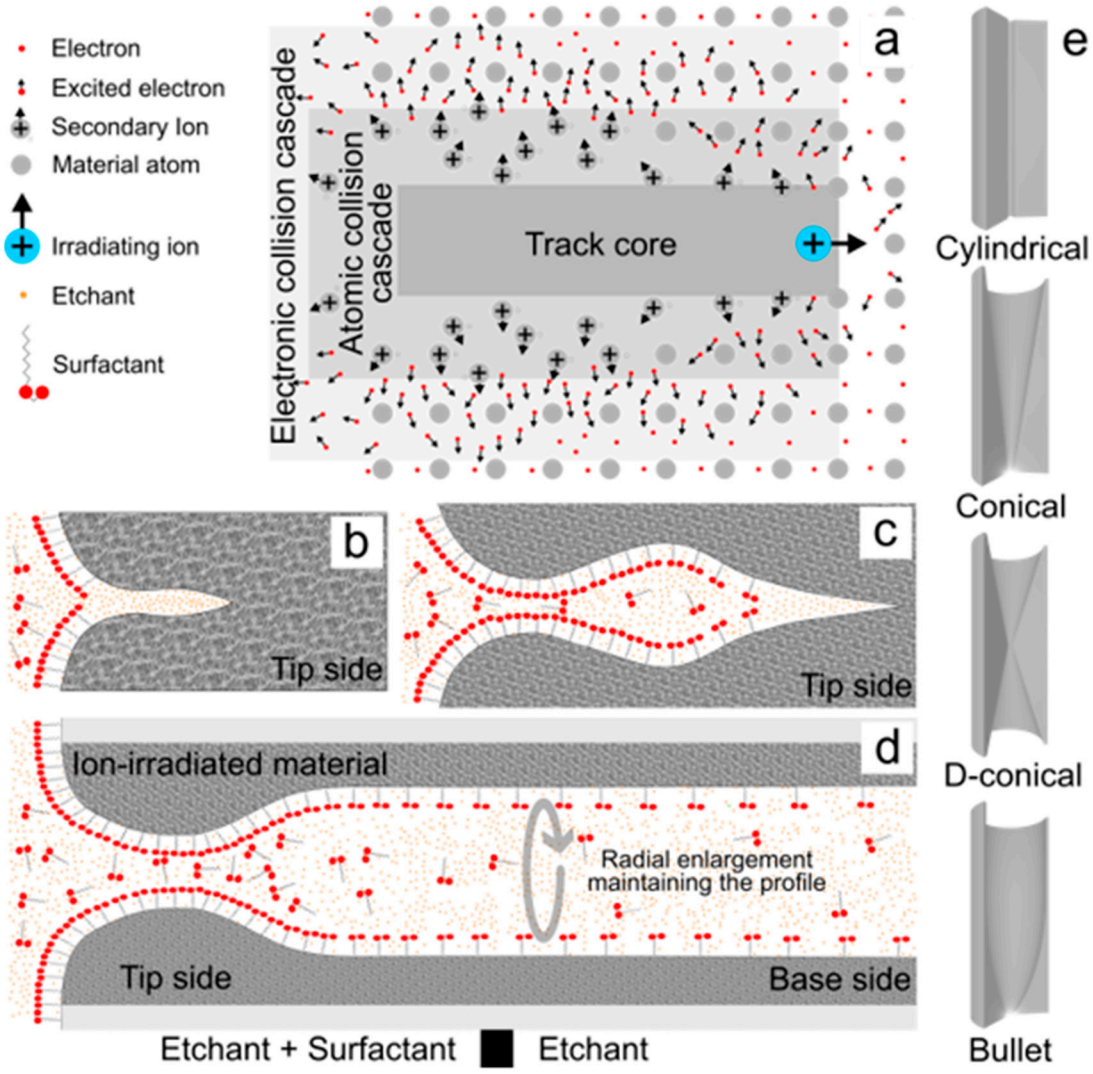

Figure 2. Single nanochannel fabrication procedure, a) Ion track; b) Etching: beginning of limited material degradation at the tip side, c) Etching: profile formation because of the protective effect of adsorbed surfactant molecules, d) Etching: radial enlargement, e) nanochannels of different shapes.

Note that similar principles can be employed to obtain many other shapes, in case of conical channels, a one-side etching procedure is used, for this purpose the etch solution is placed on one side of the membrane and a stopping solution is placed on the other side (the future tip side) aiming to the further neutralization of the etch agent. Consequently, radial growth rate becomes higher along the pore axes from the tip to the base side, leading to the desired profile (Figure 2e)[73,95]. On the other hand, double-conical ones can be obtained by two methodologies; a symmetrical etching involving the same etch solution at each side of the membrane [96,97], or a three steps procedure that entails a first fast pre-symmetrical etching from both sides without stopping solution and subsequent one-side etching of each side in the two and three steps, as was described for the conical ones [98] (Figure2e). These methods often involve on-line transmembrane electrochemical controls, as a channel diameter indirect on-line measurement and as an electro-stopping perforation tool as described elsewhere[99,100]. The use of etching solution additives as organic solvents and UV-irradiation have been also reported as mechanisms to control geometrical properties in polymeric membrane nanochannels by affecting wettability, surfactant action and polymer susceptibility to chemical degradation [70,101,102].

Table 2. Fabricated single nanochannels for enzyme integration in sensing applications.

© 2025 by the author(s). Distributed under a Creative Commons CC BY license.

Preprints.org (www.preprints.org) | NOT PEER-REVIEWED | Posted: 2 July 2025 doi:10.20944/preprints202507.0128.v1

Support	Fabrication specifications (tip side|base side) [1]	Shape	Etching time (minutes)	Etching T (°C)	Size(nm)[2] (tip/base/length)	Ref
PET	Ion track- asymmetrical chemical etching (6 M NaOH + 0.05% w/w Dowfax 2a1|6 M NaOH) 6 minutes, 60°C	Bullet	6	60	(90/600/12000)	[103]
					(76/560/12000)	[104]
					(55/500/12000)	[92]
					(60/600/12000)	[91]
					(No specified)	[90]
					(85/600/12000)	[89]
					(55/900/12000)	[88]
Si_3N_4	Photolithography- RIE -FIB Ga^+ 30 kV 1pA	Cylindrical	0.025	Ion beam	(50/50/100000)	[105]
PI	Ion track- chemical etching ($NaClO_4$ | $NaClO_4$), etching stop with addition of 1M KI	Double conical	Electrochemically controlled etching stop time	25	(25/1300/12000)	[96]
PET	Ion track-UV sensitized asymmetrical etching (1 M KCl + 1 M HCOOH|9M NaOH) etching stop with addition of 1 M KCl + 1 M HCOOH	Conical		30	(30/860/12000)	[99]
PET		Conical		25	(8/210/12000)	[106]
PET	Ion track-UV sensitized etching 35h (4 M NaOH + 0.02% v/v Dowfax 2a1|6M NaOH) etching stop with addition of 1 M HCl	Conical		60	(20/2500/12000)	[107]

Note 2. Polyethylene terephthalate (PET), polyimide (PI), focused ion beam (FIB), reactive ion etching (RIE). [1](Not applicable for double conical and cylindrical channels). [2](average diameter of different nanochannels fabricated with the same methodology).

2.1.2. Photolithography-Reactive ion Etching-FIB

Direct writing using focused ion beams (FIB) has become a widely used nanofabrication tool [108,109]. This technology was introduced during the 1970s and early 1980s following the invention of the liquid metal ion source (LMIS), driven primarily by the growing demand for advanced integrated circuit fabrication techniques[110]. FIB can be utilized to precisely fabricate nano-and microchannels in solid materials with diverse compositions, including metals, ceramics, semiconductors, and glass-based substrates. Compared to other high-energy particle beams (such as electron or photon beams) used for similar purposes, FIB offers clear advantages. Its heavier ion mass allows for higher strike energy with relatively short wavelengths, minimizing forward and back scattering, and thereby enhancing precision. Furthermore, the possibility to follow pore growing in real time by SEM or TEM techniques allows additional control over pore morphology [111,112]. A key parameter in FIB applications is the ability to precisely regulate beam size, current, and energy, to effectively remove or add material in localized zones as required[113,114]. FIB methodologies for single nanochannel production are often integrated with other nano and microfabrication techniques, as these nanochannels are typically supported in thin substrates that are part of microdevices with stringent precision requirements[114]. For example, photolithography, reactive ion etching (RIE), and FIB were combined to produce cylindrical nanochannels[105]. The process involves sequential steps, beginning with substrate preparation. Low pressure chemical vapour deposition (LP-CVD) is first used to prepare a three-layer material consisting of a silicon core (300 nm) sandwiched between two

© 2025 by the author(s). Distributed under a Creative Commons CC BY license.

Preprints.org (www.preprints.org) | NOT PEER-REVIEWED | Posted: 2 July 2025 doi:10.20944/preprints202507.0128.v1

silicon nitride (Si_3N_4) membranes (100 nm each) (Figure 3a). Subsequently, optical lithography is used to precisely define the channel's base aperture by removing the Si_3N_4 membrane on one side by reactive ion etching, to expose the underlying silicon substrate (Figure 3b,c), which is then chemically etched with potassium hydroxide (KOH) to reach the Si_3N_4 membrane on the opposite side (Figure 3d). Finally, FIB is used to create the cylindrical nanochannel through the Si_3N_4 membrane (Figure 3e).

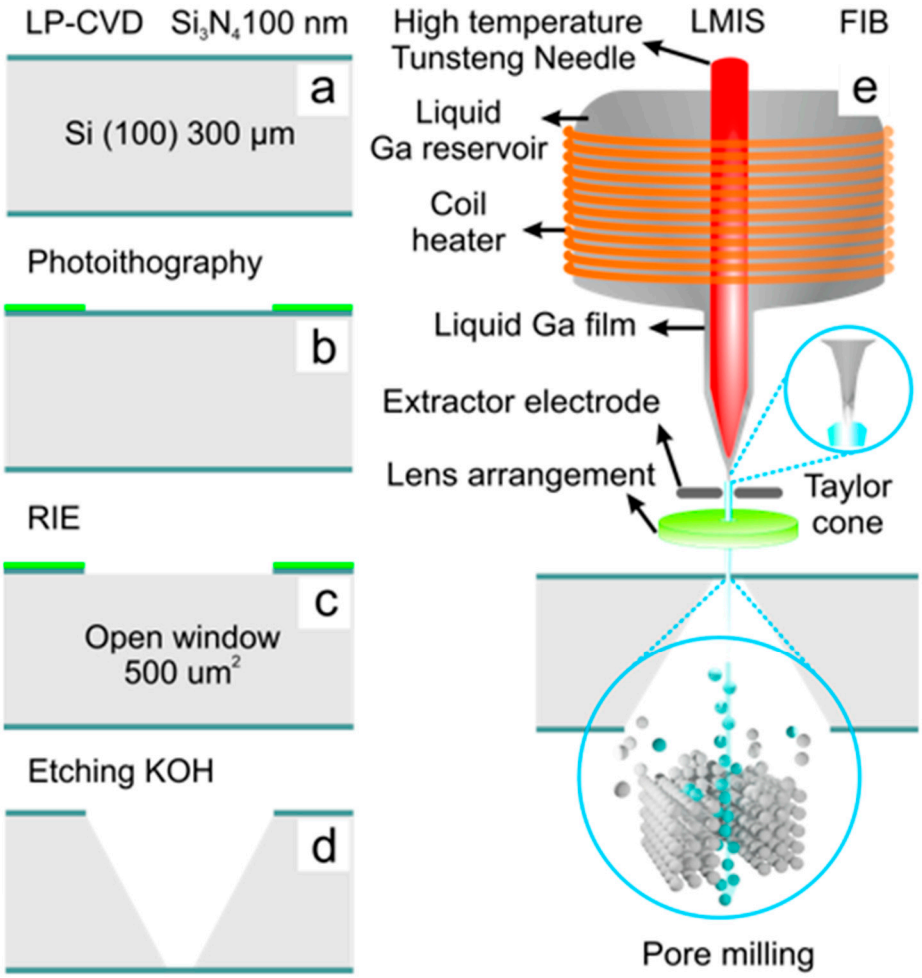

Figure 3. Photolithography-reactive ion etching-FIB nanochannel fabrication. a) Low pressure chemical vapor deposition, b) photolithography, c) Reactive ion etching, d) Selective etching, e) Liquid metal ion source for focused ion bean.

2.2. Single Nanochannel Physical and Chemical Properties

2.2.1. Morphology and Surface Chemistry

Biological channels are renowned for their structural complexity and diversity in shape and size. Their predominantly protein-based architecture provides flexibility to pore walls, enabling remarkable conformational changes in response to specific stimuli and adaptation to environmental variations. Features, such as geometry, diameter and surface chemistry have significant influence on selective chemical compound transport, water regulation, and ionic rectification[115]. These transport mechanisms, strongly influenced by channel morphology, became evident early in biological pores research and now are useful in the design and fabrication of synthetic nanopores[115]. However, single solid state nanochannels used in enzyme-based sensing applications lack of that structural flexibility at the cost of its greater chemical stability and mechanical strength. For that reason, desired size and shape must be controlled during the fabrication procedure[44,45]. As shown in Table 2, the cylindrical and double conical nanochannels are the only

© 2025 by the author(s). Distributed under a Creative Commons CC BY license.

Preprints.org (www.preprints.org) | NOT PEER-REVIEWED | Posted: 2 July 2025 doi:10.20944/preprints202507.0128.v1

symmetric designs employed. In contrast to the asymmetric bullet-shaped and conical-shaped nanochannels, the cylindrical design features an almost uniform diameter along its entire length, whereas the double conical design is characterized by two opposing, gradually tapering conical sections that converge at the central region, forming the narrowest point. These structural features, combined with the greater length of the cylindrical channel, influence the transduction mechanisms, as described below[34]. The inner surface chemistry of nanochannels is another critical parameter in channel sensor development. The functional chemical groups exposed on the surface after pore formation depend on the composition of the support material and significantly influence ion transport mechanisms in unmodified channels. Moreover, subsequent surface modifications depend on the availability of chemical anchor points[84,86].

Polyethylene terephthalate and polyimide (Kapton) have been extensively utilized as base materials for single and multi-nanochannel arrays in membrane technology due to their advantageous properties[30,70,116]. Both materials share excellent chemical stability, relatively low dielectric constants, insulating nature, and high mechanical strength. However, PI is recognized for its superior performance compared to PET. This performance advantage comes at the cost of a more intricate chemical synthesis process, which translates into higher production expenses. Furthermore, the enhanced resistance of PI presents additional challenges during the etching process, hot concentrated sodium hypochlorite solutions are often used because certain etchants may become unstable at the elevated temperatures required for processing this material[70]. Silicon nitride is also widely recognized for its excellent mechanical, thermal, and chemical resistance, making it highly suitable for applications subjected to high temperatures and stress[117]. This durability enables it to withstand FIB and EB fabrication techniques without catastrophic structural failure (Table 1). Chemical etching has also been employed for channel fabrication in Si_3N_4 membranes. However, due to its robust properties, more stringent conditions are required to generate nanopores via chemical etching. For example, a study reports the treatment of a thin silicon nitride membrane with concentrated HF or H_3PO_4 solutions at 150 °C for over 20 minutes to achieve channels with base diameters under 100 nm[74].

Figure 4 illustrates the chemical structures and precursors of PET (a) and PI (b). The synthesis of these polymers is achieved through condensation reactions: terephthalic acid reacts with ethylene glycol to form PET, while pyromellitic dianhydride reacts with 4,4'-diaminodiphenyl ether to produce PI[70,118]. During the etching process, basic hydrolysis of these materials generates abundant carboxylate terminal surface groups (-COO^-). In the case of PI, amine terminal groups (-NH_x) can also be formed on the etched surface[73,118–120]. These chemical terminations act as anchor points for subsequent surface modification, enabling techniques such as direct chemical attachment or electrostatic self-assembly, as demonstrated in various studies (Table 4). On the other hand, Si_3N_4 based channels, due to their less versatile surface chemistry dominated by SiO_2 groups after FIB fabrication, require additional preconditioning for effective integration of functional structures. For instance, as reported in[105], a hydroxylation treatment with H_2SO_4/H_2O_2 followed by silanization with APTES was employed to introduce amine terminal groups, enabling further surface modification[121](Figure 4c).

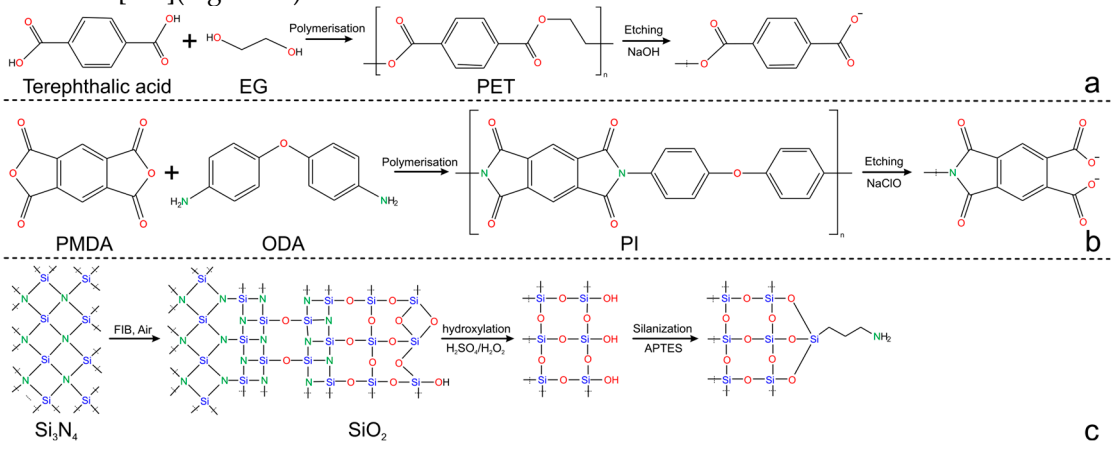

© 2025 by the author(s). Distributed under a Creative Commons CC BY license.

Preprints.org (www.preprints.org) | NOT PEER-REVIEWED | Posted: 2 July 2025 doi:10.20944/preprints202507.0128.v1

Figure 4. The chemistry of etching of different membrane materials: a) PET, b) PI, c) Si_3N_4.

2.2.2. Wettability

Fluids exhibit complex and often unexpected behaviors in nanoscale environments. In particular, wetting behavior of water in nanoconfined spaces plays a crucial role in matter transport and signal transmission in biological systems[122,123]. Many protein channels utilize gating mechanisms based on wetting and dewetting processes to effectively regulate ions and small neutral molecules flux[124,125]. Since water serves as the primary solvent in biological systems, solutes cannot pass through dry (dewetted) pores. A key factor in regulating wettability within water channels is the hydrophobicity of the pore walls. It has been demonstrated that uncharged surfaces within nanochannels promote water evaporation, resulting in the formation of local vapor pockets. This leads to a non-conductive (closed) state at which no transport occurs[126]. Additionally, studies have shown that even in channels with low surface charge, a closed state is observed when the channel diameter falls below 20 nm[127]. These insights highlight the importance of wettability as a critical parameter in the development of single nanochannel enzymatic biosensors. Since biosensing mechanisms depend on continuous mass transport through the channel to facilitate enzyme-substrate interactions, physicochemical transduction processes and ionic current measurements, maintaining the conductive (open) state is essential. Consequently, hydrophilic channels with larger diameters and highly charged surfaces are preferred to ensure optimal functionality.

2.3. Transport in Single Nanochannels

'*There is plenty of room at the bottom*,' were the iconic words of Professor Richard Feynman, highlighting the vast potential to decipher and mimic the complex processes taking place in biological systems at the micro- and nanoscale[128]. Although he was not referring to physical space, it is interesting that a deeper understanding of these processes has revealed that, in the case of pores and nanochannels, reduced space is the key factor underlying the unique physicochemical mechanisms governing matter transport. For example, in biological channels with effective diameter below 10 nm, the confined size has significant implications on the regulation of water-, ions-, and neutral molecules transport through them[129]. At the nanoscale, interactions that are negligible in bulk volumes become dominant, while conventional bulk laws lose influence as dimensions decrease[130,131].

2.3.1. The Nanoconfinement Effects

Beyond the influence of surface physicochemical properties on various processes occurring in nanochannels, nanometric confinement itself acts as a powerful regulator of multiple physical and chemical phenomena. For instance, it has been reported in theoretical and experimental studies that acid-base equilibria can shift significantly when dissociable groups are confined at the nanoscale, primarily due to repulsion effects arising from restricted space[132–134]. Additionally, it was observed that electrostatic self-assembly of polyelectrolytes behaves differently inside nanochannels compared to bulk surfaces, with these deviations attributed to the distinct structural organization that polymers adopt under nanoconfinement[135,136]. Similarly, crystallization, precipitation, and adsorption processes are influenced by nanoscale confinement, leading to phenomena such as the formation of metastable crystalline phases not observed in bulk systems, localized precipitation/dissolution gating mechanisms, and preferential adsorption[137–139]. Enzyme activity is also affected at this scale, though responses vary depending on the specific system. Some studies report a reduction in activity due to steric hindrance, whereas other studies observe an enhancement attributed to shorter substrate diffusion distances[140,141]. In terms of sensing performance, most single nanochannel-based systems exhibit linear detection zones in the nano- to micromolar range. This sensitivity is largely attributed to the concentration effect caused by species accumulating in the femtoliter-sized volumes within the narrowest sections of the channel. Additionally, at these shorter

© 2025 by the author(s). Distributed under a Creative Commons CC BY license.

Preprints.org (www.preprints.org) | NOT PEER-REVIEWED | Posted: 2 July 2025 doi:10.20944/preprints202507.0128.v1

distances, both substrate-enzyme interactions and the coordinated functions among functional elements are enhanced, further improving sensing performance.

2.3.2. Forces Regulating Ion Behavior

Due to the continuous increase in the surface-to-volume ratio, interfacial effects such as steric interactions and hydration (~1–2 nm range), Van Der Waals forces (~1–50 nm range), and electrostatic interactions (~1–100 nm range) gain crucial importance in nanoconfined spaces[142]. Phenomena such as ultrafast liquid flow, ion rectification, nanoprecipitation, nanoevaporation, and polarization concentration deviate considerably from bulk behavior, necessitating approaches beyond classical theories to accurately explain them[143,144]. In this section, we will discuss some of the most widely accepted models used for this purpose, focusing on those that help elucidate the elegant transduction mechanism converting chemical processes into a measurable electrical response. Models based on evaporation and pressure-driven flow will not be considered here as they are not relevant for enzyme-based sensors; for a detailed description of general transport phenomena in nanometric and sub-nanometric structures, the reader is referred to[142,145–147].

As mentioned above, water remains essential as a medium for matter transport at these scales. Consequently, a nanochannel placed between two bulk reservoirs, that is completely filled with an aqueous electrolyte solution will be considered, and the non-conductive state resulting from drying is disregarded (Figure 5a). Given the high sensitivity of electrostatic charges to changes in solution pH, the inner channel surface acquires an electrostatic charge as described by Equation 1 (given in C m^{-2}), due to the dissociation of groups on the inner wall and/or the specific non-electrostatic adsorption of ions from the solution[148–151] (except at the point of zero charge, when electroneutrality is reached at a specific pH). It will be shown that the presence of surface charges has significant implications on transport.

$$\sigma_s = \sum_i F\Gamma_i q_i \quad (1)$$

Where $q_i = z_i e$ is the net charge of *i*, *z* is the valence of ion *i*, *e* is the electron charge (1.602*10^{-19} C), and Γ_i is the surface density of *i* ($mol\ m^{-2}$), F is the Faraday constant.

When fixed charges are present on the channel wall, counterions migrate from the bulk to restore electroneutrality, resulting in the formation of a screening cloud composed of regions with varying ionic concentration and mobility, collectively known as the electrical double layer (EDL). The EDL is typically divided into two main zones: a compact layer (Stern layer) of counterions with limited mobility immediately adjacent to the channel wall, next to a diffuse layer (Gouy-Chapman layer) where the concentrations of ions and counterions decay exponentially toward the bulk[152,153] (Figure 5b). The thickness of the EDL depends on both the surface charge density and the electrolyte concentration. For instance, at high electrolyte concentration or low surface charge density, the screening cloud is thin because the potential generated by the fixed charges has only a short-range effect. Conversely, at high surface charge density or low electrolyte concentration, the EDL extends further into the solution[146,154]. The electrostatic potential profile in space, arising from the charge distribution at the solid-liquid interface, is described by the Poisson-Boltzmann equation (Figure 5c).

$$\nabla^2\psi = \frac{e}{\varepsilon_0\varepsilon_r}\sum_i n_i^{\infty} z_i exp\left[\frac{-z_i e\psi(x)}{k_B T}\right] \quad (2)$$

Where ψ is the electric potential (V) due to the surface charge, ε_0 is the vacuum permittivity (8.854*10^{-12} F m^{-1}), ε_r is the relative permittivity, e is the electron charge, z_i is the valence of i, n_i^{∞} is the bulk volume density, x is the spatial coordinate perpendicular to the charged plane surface (m), k_B is the Boltzmann constant (1.381*10^{-23} J K^{-1}), T is the absolute temperature (K).

This equation can be solved analytically by assuming a small surface potential in the EDL ($z_i\psi$<0.0257 V at 25 °C) and expanding the exponential function using the first-order linearization $e^{-\alpha} = 1 - \alpha$ for small α. This leads to the Debye-Hückel approximation (Equation 3), where the κ parameter, defined as the Debye-Hückel parameter is related to the Debye length (λ_D), which corresponds to a measure of the thickness of the EDL $\lambda_D = \kappa^{-1}$ [155,156].

$$\nabla^2\psi = \kappa^2\psi(z) \quad (3)$$

© 2025 by the author(s). Distributed under a Creative Commons CC BY license.

Preprints.org (www.preprints.org) | NOT PEER-REVIEWED | Posted: 2 July 2025 doi:10.20944/preprints202507.0128.v1

being $\kappa = (\frac{e^2 \sum_i n_1^{\infty} z_i^2}{\varepsilon_0 \varepsilon_r k_B})^{\frac{1}{2}}$

For a symmetric $z_i : z_i$ electrolyte in water at 25 °C, λ_D (nm) can be calculated using Equation 4. Under these conditions, the electric potential extends approximately $3\lambda_D$ before decreasing to about 2% of its initial value. Considering the typical EDL thicknesses in KCl solutions (Table 3), it is evident that for concentrations below 1 mM, the surface charge-induced potential variation can extend up to 30 nm from the surface. Consequently, in a nanochannel with a diameter of ~60 nm, the entire radial aperture will be influenced by the EDL potential (Figure 5a)[145].

$$\lambda_D = \frac{0{,}215}{\sqrt{I_s}} \quad (4)$$

Where I_s is the ionic strength, defined as $I_s = \frac{1}{2} \sum c_i z_i^2$

Table 3. Debye length λ_D in usual KCl solutions calculated from equation 3, based on the approximation ($z_i \psi$<0.0257 V at 25 °C).

KCl (M)	Debye length λ_D (nm)
10	0.3
10^{-1}	1.0
10^{-2}	3.1
10^{-3}	9.6
10^{-4}	30.5
10^{-5}	96.3

© 2025 by the author(s). Distributed under a Creative Commons CC BY license.

Preprints.org (www.preprints.org) | NOT PEER-REVIEWED | Posted: 2 July 2025 doi:10.20944/preprints202507.0128.v1

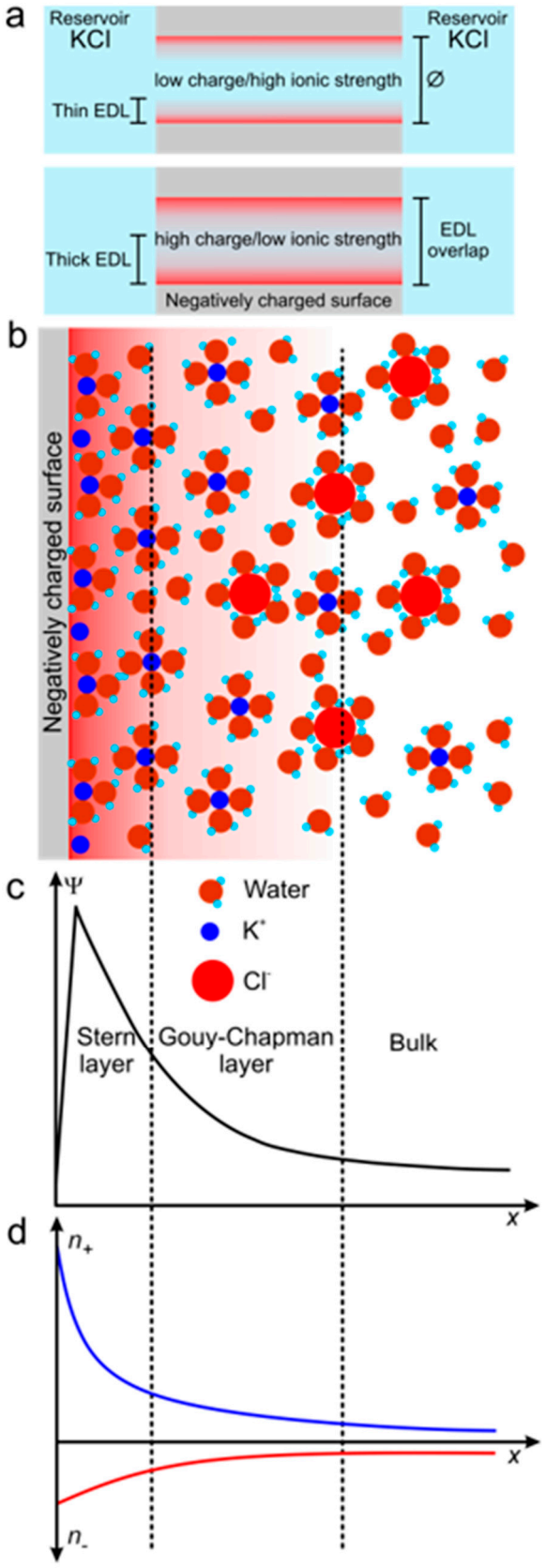

Figure 5. The electrical double layer (EDL). a) Electrical double layer length in low and high surface charge or ionic strength solutions. b) Scheme of the ion distribution at the EDL. c) Potential distribution as a function of the distance to the charged surface. d) ion concentration profiles from the charged surface. .

Although the Debye screening model is useful for describing symmetric electrolyte distributions at low surface potential and enables the calculation of key EDL parameters, it has limitations when

© 2025 by the author(s). Distributed under a Creative Commons CC BY license.

Preprints.org (www.preprints.org) | NOT PEER-REVIEWED | Posted: 2 July 2025 doi:10.20944/preprints202507.0128.v1

accurately representing high surface potential distributions or distinguishing the individual contributions of ions and counterions to charge balance in asymmetric electrolyte systems. To overcome these limitations, the Gouy-Chapman model, derived from a numerical solution of the Poisson-Boltzmann equation, is used[154,157]. This model demonstrates that charge balance is predominantly achieved through counterion accumulation at the interface (Figure 5d). As a result, the ionic concentration in the EDL cloud is significantly higher than in the bulk[158]. This effect plays a crucial role in the high surface conductance observed at charged interfaces in an electrostatic aqueous medium when an electric field is applied. The electric field overcomes the attractive electrostatic force between counterions and the charged surface, inducing the movement of the accumulated ions. This motion, in turn, drags water and neutral solutes along the direction of the ionic flux, thereby facilitating and enhancing matter transport[159,160].

Note that liquid, solute and ion transport are strongly coupled at the nanoscale. Although concentration gradients can drive osmotic flow, during single nanochannels sensing, the bulk reservoirs composition is generally symmetric, and changes in concentration of uncharged substrates during measurement by enzyme reactions are not enough to generate a measurable flux. Therefore, electro-osmotic flow by voltage gradient is the governed regime of transport in these systems[143,145,161].

2.3.3. Signal Sources in Nanochannels: Iontronic Current, ICR and TEs

A basic understanding of the forces responsible for ionic movement at interfaces with dimensions comparable to the Debye length has been briefly summarized from the perspective of the channel wall because this viewpoint highlights the direct influence of surface charges on the local ionic environment. Now, let us review the models used to describe ion concentration distribution and ionic current throughout the entire nanochannel. For instance, let us consider the same cylindrical channel with a diameter of 60 nm in a 1 mM KCl solution (Figure 5a). In this scenario, the surface charge directly influences the overall potential distribution; consequently, it also governs the ion concentration inside the channel, which in turn affects the ionic current[162,163]. Under these conditions—characterized by high surface charge or low salt concentration—the ion concentration inside the channel is higher than in the bulk electrolyte[164]. This occurs because counterions accumulate inside the channel to neutralize the fixed surface charge, while co-ions amount also increases in the diffuse layer due to satisfied electroneutrality. This concentration imbalance, known as the excess mobile counterion concentration $c_e = \frac{2\sigma_s}{rN_Ae}$ is a concentration threshold that must be considered to obtaining the model for nanochannel conductance (G) (Equation 5)[143]. This approximation accounts for the fact that at ionic strengths higher than c_e, conductance primarily depends on the channel geometry (first term). However, at ionic strengths lower than c_e, surface charge dominates the conductance, making it less dependent on the geometrical factor (second term), it is important to highlight that, although this equation refers to a symmetric cylindrical nanochannel behaving similarly to an ohmic resistor, the same principle applies to asymmetric ones as well[145].

$$G = (\mu_{K^+} + \mu_{Cl^-}) n_{KCl} e \frac{\pi r^2}{l} + 2\mu_{K^+}\sigma_s \frac{2\pi r}{l} \quad (5)$$

Where σ_s is the surface charge, μ Is the mobility ($m^2\ V^{-1}\ s^{-1}$) and n is the volume density (m^{-3}), r is the radius (m) and l is the length of the nanochannel (m).

The conductance of a single SSN nanochannel is defined as $G = \frac{I}{\Delta V}$. I/V curves are obtained by applying a DC voltage and recording the steady-state current using the setup shown in (Figure 6a). The silver-silver chloride (Ag|AgCl) electrode is commonly used in nanofluidic measurements due to its stability, non-polarizability, and minimal capacitive effect[143]. These properties are essential, as the electrodes are responsible for both current measurement and voltage application. A typical I/V curve recorded with a symmetrical cylindrical nanochannel exhibits a straight line with slope G, characterized by identical absolute current values for voltages of equal magnitude but opposite polarity. As the geometry and surface charge are symmetrical across the channel, the electrostatic potential and ionic cloud are also homogeneously distributed. Consequently, the channel exhibits

© 2025 by the author(s). Distributed under a Creative Commons CC BY license.

Preprints.org (www.preprints.org) | NOT PEER-REVIEWED | Posted: 2 July 2025 doi:10.20944/preprints202507.0128.v1

ohmic behavior, at which the current varies linearly with the applied voltage[144,165](Figure6b). It is important to note that no faradaic processes occur in this system; therefore, the recorded signal arises solely from ion migration. As a result, this output is referred to as an iontronic current, which, at these conditions, depends strongly on the surface charge. This characteristic makes it inherently useful as a response variable in sensing applications, as any physicochemical process that modifies the surface charge can be detected through changes in the iontronic output[43–45,166].

Figure 6c presents a different system where the I/V curve is recorded using an asymmetrical bullet-shaped nanochannel. Due to the broken geometrical symmetry, the potential distribution is no longer homogeneous across the channel volume, leading to special transport regimes[167]. Note that our previous discussion on surface charge control over ion transport applies primarily to the narrow tip region (~60 nm). As the channel widens toward the base (~700 nm), the electric double layer loses influence over ion transport due to its limited extension relative to the channel diameter. When a +1V potential is applied to the electrode near the tip of a negatively charged channel, an ionic current (I) is recorded. However, when the polarity is reversed (-1V), the net ionic current decreases significantly, often by several orders of magnitude (Figure 6c, red curve). This phenomenon, known as ion current rectification (ICR), has been extensively studied in previous works[146,168,169]. Briefly, EDL overlaps at the channel tip enhances counterion permeability while hindering the flow of co-ions[131]. This results in an ionic accumulation/depletion mechanism governed by the applied potential polarity, producing a diode-like behavior, characterized by a high and a low conductance branch in the I/V curve. ICR is a fundamental mechanism in enzyme biosensing with single nanochannels, as most nanochannels used in these applications feature asymmetric potential distributions (Table 4).

Similar to the iontronic output in symmetrical systems, ICR is highly sensitive to surface charge changes[162,170]. Thus, the rectification efficiency (f_{rec}), defined as the ratio of the current in the high-conductance state to that in the low-conductance state at a fixed voltage, serves as a key response variable. Moreover, ion current rectification enables the qualitative characterization of the nanochannel's electrostatic surface charge properties, as both cation-driven and anion-driven rectification can be achieved and distinguished within the same channel, depending on surface charge polarity. Notably, the broken symmetry required for ICR can result not only from asymmetric geometry but also from asymmetric surface charge modifications or from the presence of different electrolyte solutions in the reservoirs[171].

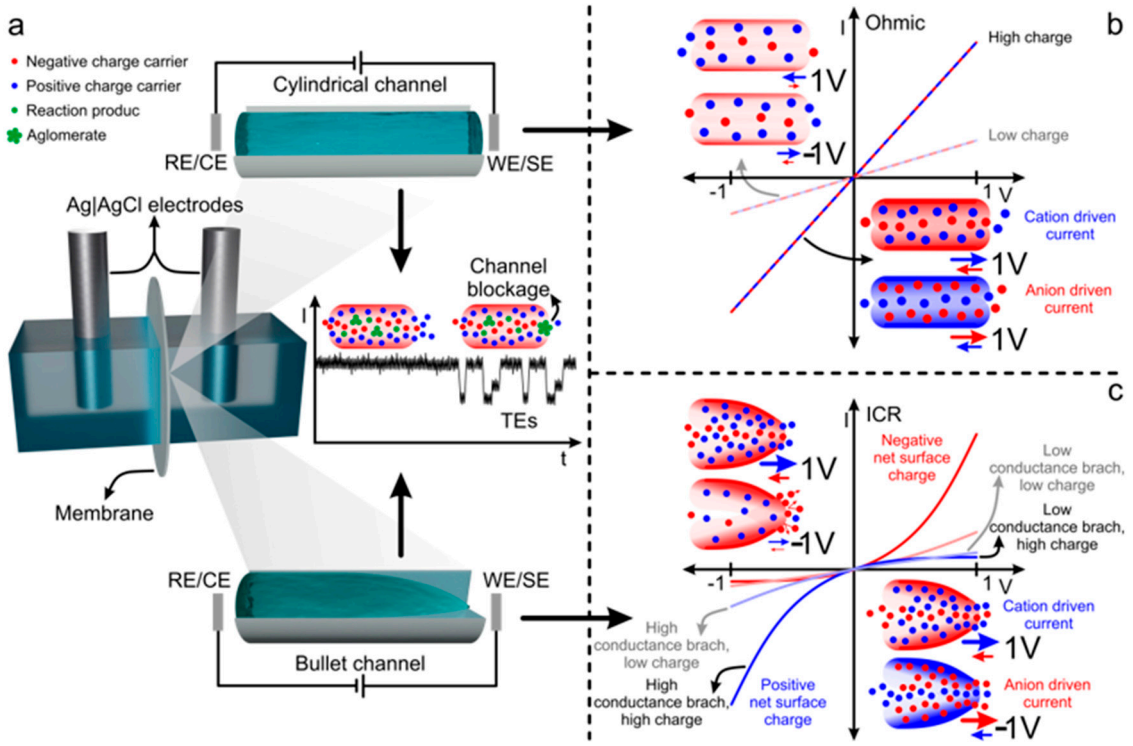

© 2025 by the author(s). Distributed under a Creative Commons CC BY license.

Preprints.org (www.preprints.org) | NOT PEER-REVIEWED | Posted: 2 July 2025 doi:10.20944/preprints202507.0128.v1

Figure 6. Iontronic current measurement. a) Measurement setup and representation of translocation events (TEs) that can be observed in symmetric and asymmetric nanochannels. b) Iontronic ohmic response in symmetric nanochannels with high and low net surface charge. c) Ion current rectification in bullet-shaped nanochannels, cation- and anion-driven rectification.

The physical analysis of transport phenomena in nanochannels has been approached from different perspectives, each successfully explaining experimental results and predicting ionic current responses under specific system conditions[172]. In the case of single nanochannels embedded in polymeric membranes, the Poisson–Nernst–Planck (PNP) model is widely employed to describe I/V curves and ion current rectification properties. Furthermore, it allows for the prediction of ion concentration profiles and electric potential distribution within the channel. Since obtaining analytical solutions for the 3D PNP model will not be possible, simplified 1D equations are typically used. The ionic flux for each species is described by the Nernst–Planck equation (Equation 6), while the relationship between electric potential and ion concentration is governed by Poisson equation (Equation 7). Finally, the Navier–Stokes equation accounts for the flow distribution, incorporating both pressure-driven and electrokinetic contributions (Equation 8). To fully define the system, numerical solutions e.g. using finite-difference or finite-element methods with appropriate boundary conditions considering steady-state conditions $\nabla j_i = 0$ and incompressible fluid flow $\nabla u = 0$ [173,174].

$$J_i = -D_i \nabla c_i - \frac{z_i F}{RT} D_i c_i \nabla \Phi + c_i u \quad (6)$$

$$\nabla^2 \Phi = -\frac{F}{\varepsilon} \sum z_i c_i \quad (7)$$

$$u \nabla u = \frac{1}{\rho} (-\nabla \mathrm{P} + \eta \nabla^2 u - F(\textstyle\sum_i z_i c_i) \nabla \Phi) \quad (8)$$

Where J_i, D_i, c_i, and z_i are respectively, the flux (mol s^{-1} m^{-2}), diffusion coefficient (m^2 s^{-1}), concentration, and charge of species i. Φ and u are the total electric potential (V) and fluid velocity (m s^{-1}), and F, R and T are Faraday constant, the gas constant and the absolute temperature, respectively. ε is the dielectric constant, ρ is the density (kg m^{-3}), η is the viscosity of the fluid (kg m^{-1} s^{-1}) and P is the pressure (N m^{-2}).

Another important mechanism of response modulation in both symmetrical and asymmetrical systems is the variation of the effective channel size. Since the iontronic signal depends on ion transport, any variation in the cross-section area inside the channel will be reflected in changes in the net recorded current. Partial or total channel blockage—or conversely, unblocking—can result from analyte attachment or release, reorganization of supramolecular structures on the surface, or the passage of large molecules or particles through the channel. This sensing strategy has been less explored in single nanochannel enzyme biosensors. However, translocation events (TEs) associated with a partial reduction in the effective channel size have been also used as a signal correlated with analyte concentration[175].

3. Sensing Platform Nanoarchitecture

A bare nanochannel alone can serve as a valuable tool for ion sensing; however, uncharged biomarker molecules typically pass through undetected at clinically relevant concentrations, unless they are exceptionally large (e.g., macromolecules such as proteins, RNA, or DNA). As observed in nature, achieving specificity and sensitivity in detection or regulation of a particular substrate requires a well-organized assembly of functional elements operating in concert[176,177]. Therefore, the design and construction of biomimetic sensing platforms must incorporate a similar level of structural organization. In this section we will review the architecture of biosensing single nanochannel systems, focusing on the integration of recognition, signal transduction, and amplification elements onto the channel wall and how their coordinated functions allow the transformation of substrate amount into measurable current.

3.1. Functional Blocks Integration

© 2025 by the author(s). Distributed under a Creative Commons CC BY license.

Preprints.org (www.preprints.org) | NOT PEER-REVIEWED | Posted: 2 July 2025 doi:10.20944/preprints202507.0128.v1

3.1.1. One Block Systems

As explained in Section 2.2 and illustrated in (Figure 4), the availability of reactive chemical groups after nanochannel fabrication serves as anchoring sites for the integration of subsequent building blocks. Although most reported systems incorporate transduction-amplification elements in addition to the nanochannel wall itself, some studies have demonstrated that a recognition element alone (one block) can suffice for substrate sensing. In this simple architecture one or more enzymes are directly immobilized on the surface via covalent coupling through the well-established EDC-NHS zero-length crosslinking methodology[96,99,105,107]. Briefly, EDC reacts with carboxyl groups to form a highly reactive O-acylisourea intermediate, which readily undergoes nucleophilic addition. To prevent hydrolysis, NHS is introduced, forming a semi-stable N-hydroxysuccinimidyl (NHS) ester. Finally, primary amine groups from enzymes react with the NHS-ester, generating a stable amide bond that covalently links the enzyme to the surface [178,179](Figure 7a,b). Simplicity and effective immobilization are the main advantages of this methodology; however, it has been reported that enzyme activity can be affected by active site blockage or structural alterations resulting from covalent bond formation.

3.1.2. Two Blocks System

Platforms incorporating additional transduction-amplification elements (two-blocks systems) introduce an extra constructional block aimed at enhancing overall performance and expanding the possibilities for recognition element attachment. While these systems are more complex than single-block configurations, their complexity varies depending on the number of layers of a specific block incorporated. For instance, different designs have been developed by alternating one, two, three, or four layers of each block. Among the additional blocks reported to date, cationic polyelectrolytes have been the most widely employed (Table 4). These large polymer chains provide a high density of cationic charges with diverse acid-base equilibrium constants and enable enzyme immobilization through simple layer-by-layer electrostatic self-assembly[88–92]. Although the exact procedure depends on the specific polyelectrolyte or enzyme used, the general methodology involves the initial self-assembly of a polyelectrolyte layer at a specific pH, ensuring a positively charged polymer and a negatively charged bare pore wall. The modified channel is then exposed to an enzyme-containing solution at an optimized pH to promote electrostatic interactions. This process can be repeated as needed to achieve the desired number of layers for each block (Figure 7d,e). Despite not requiring complex chemistry, these procedures demand precise pH control and, in some cases, extended fabrication times. Additionally, since electrostatic interactions depend on surface charges, these architectures exhibit high pH sensitivity. Regarding catalytic performance, enzyme immobilization via electrostatic self-assembly onto polyelectrolyte surfaces has been reported as one of the methods with minimal impact on enzymatic activity[180,181]. This is attributed to the intrinsic ability of polymers to reorganize their structure and the absence of covalent bond formation, which helps preserve enzyme functionality[182,183].

A recent approach reported by Huamani et al. introduces a novel procedure that incorporates a one-pot metal-organic framework (MOF) as a structural component. This porous framework serves as a source of positive charge groups due to the presence of Zr^{4+} ions and amino functional groups. Additionally, the amino groups act as anchor points for subsequent enzyme attachment. The immobilization strategy utilizes divinyl sulfone (DVS) as a cross-linking agent to covalently bind urease to the amino-functionalized UiO-66-NH_2 framework (Figure 7c). DVS is a bifunctional electrophilic agent that reacts with amines, thiols, and hydroxyls under mild aqueous conditions, forming stable sulfonate linkages[184–186]. This enables the formation of robust MOF-DVS-enzyme covalent bonds through a two-step anchoring process. First, the nanochannel wall is activated with DVS, and subsequently, the pre-activated surface is exposed to an aqueous enzyme solution. This method offers advantages such as mild reaction conditions and enhanced structural stability, thereby expanding the operational range of the sensing platform. However, one-pot MOF synthesis is a labor-

© 2025 by the author(s). Distributed under a Creative Commons CC BY license.

Preprints.org (www.preprints.org) | NOT PEER-REVIEWED | Posted: 2 July 2025 doi:10.20944/preprints202507.0128.v1

intensive procedure, requiring specific nanochannel preconditioning as well as precise control over temperature and pressure conditions[103].

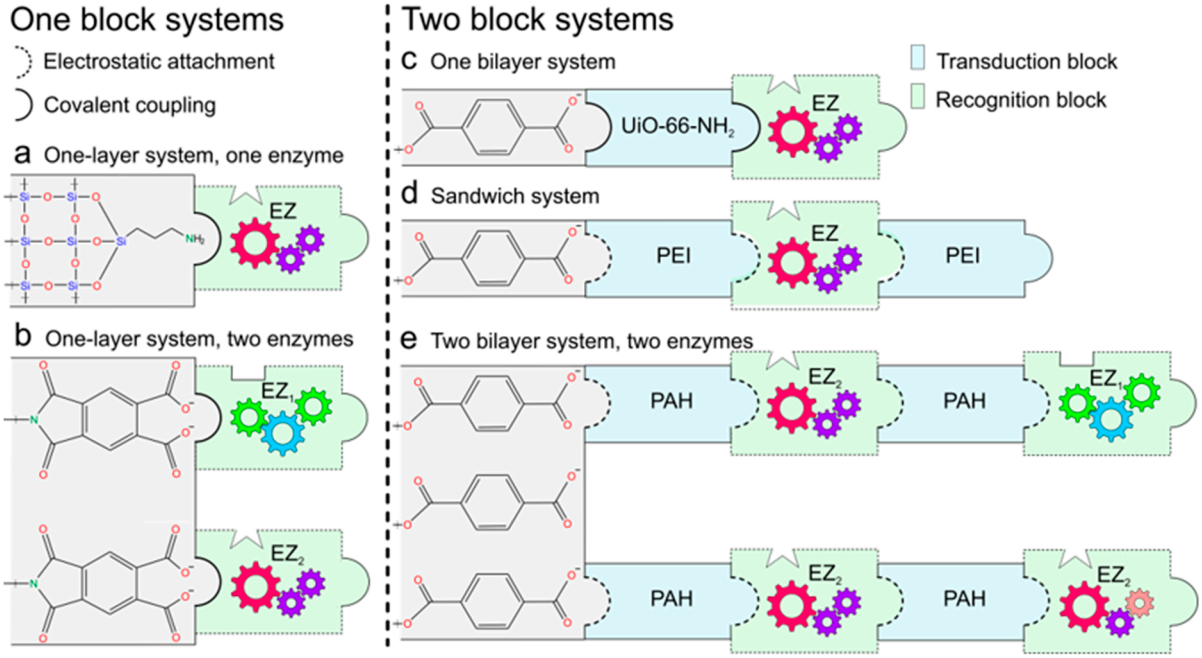

Figure 7. Platform architecture a) One-block system: An enzyme layer is immobilized on the surface via a covalent bond. b) One-block system: A multi-enzyme layer is integrated via covalent bonding. c) Two-block system: A metal-organic framework (MOF) layer is integrated as an amplification and immobilization block. The enzyme layer is covalently attached. d) Two-block system: The enzyme is electrostatically sandwiched between two polyelectrolyte layers. e) Two-block system: Polyelectrolyte/enzyme layers are electrostatically attached.

Table 4. Single nanochannels enzyme-based biosensors nanoarchitectonics.

Building blocks layers	**Blocks Integration**	**Transduction mechanism**	**Ref**
UiO-66-NH_2-Urease	One-pot MOF synthesis, DVS-mediated crosslinking by Drop-coating	pH change effect over f_{rec}, single reaction	[103]
PAH/ADA/PAH	Layer by layer self-assembly by Dip-coating and Drop-coating	pH change effect over f_{rec}, single reaction	[104]
PAH/Urease/PAH/Urease: Arginase	Layer by layer self-assembly by Dip-coating	pH change effect over f_{rec}, cascade concerted functions	[92]
PEI/CD/PEI	Layer by layer self-assembly by Dip-coating and Drop-coating	pH change effect over f_{rec}, single reaction	[91]
PAH/Urease	Layer by layer self-assembly by Dip-coating	pH change effect over f_{rec}, steric obstruction	[90]
PEI/AchE	Layer by layer self-assembly by Dip-coating and Drop-coating	pH change effect over f_{rec}, single reaction	[89]
PAH/Urease	Layer by layer self-assembly by Dip-coating	pH change effect over f_{rec}, single reaction	[88]
HRP	EDC-NHS covalent coupling	Translocation events ($ABTS^{\bullet+}$ aggregates)	[105]

© 2025 by the author(s). Distributed under a Creative Commons CC BY license.

Preprints.org (www.preprints.org) | NOT PEER-REVIEWED | Posted: 2 July 2025 doi:10.20944/preprints202507.0128.v1

GOx/HRP		pH change influence over transmembrane current-cascade concerted functions	[96]
GOx		pH sensitive, single reaction	[99]
HRP		Steric obstruction, specific interaction	[106]
HRP		$ABTS^{\bullet+}$ sensitive, electrostatic interaction and steric obstruction	[107]

Note 3. Polyethylene terephthalate (PET), polyimide (PI), Silicon nitride (Si_3N_4), Polyallylamine hydrochloride (PAH), Polyethyleneimine (PEI), Adenosine deaminase (ADA), Creatinine deaminase (CD), Acetylcholinesterase (AchE), Horseradish peroxidase (HRP), poly-L-Lysine (PLL), Glucose oxidase (GOx), Rectification factor (f_{rec}).

3.2. Recognition and Transduction Mechanism

The transduction mechanism in reported single-block platforms follows two distinct pathways, depending on the specific system. The first mechanism arises from the incorporation of enzyme electrostatic charge groups into the overall surface charge distribution upon immobilization. Since proteins structure contains amino acids with amphoteric functional groups, the net surface charge results from the balance of the entire charge cloud under specific environmental conditions, effectively functioning as a supramolecular amphoteric arrangement. In this context, the presence of charged groups or charged substrates can modify the net surface charge, consequently altering ion concentration within the EDL, which leads to variations in the recorded current. Thus, the generation of new charged species due to pH fluctuations or chemical reactions is sensitively transduced into changes in the I/V response (Figure 8a) [47,187]. The second transduction pathway involves a reduction in the effective channel size. In this case, partial and transient obstruction at the channel tip occurs due to the passage of small agglomerates formed within the channel as a result of nanoconfinement-driven accumulation of reaction products. When the channel aperture is temporarily narrowed, a translocation event (TE) is recorded as a spontaneous decrease in current (Figure 8b). The frequency and amplitude of these TEs depend on the applied potential; however, by setting a defined bias, a correlation with substrate concentration has been reported, enabling indirect analyte determination. It is important to clarify that the simplicity of single-block platforms, as previously mentioned, refers to their construction rather than their sensing mechanism. In fact, both transduction mechanisms can coexist within the same system, and complex concerted cascade enzymatic reactions may be required for the detection of specific analytes [105,107,188,189].

Beyond the assembly advantages provided by the integration of additional blocks in two-block systems, certain functional properties are also enhanced. For instance, in platforms exhibiting ICR, the presence of additional charges with opposite polarity enables both cationic and anionic driving sensing signals due to a broader distribution of pH-sensitive charges. In contrast, single-block systems typically allow only cation- or anion-driven signals recording. This enhancement in pH response not only broadens the substrate detection range but also improves sensitivity and detection limits in some cases. The transduction mechanisms in two-block systems are generally based on the same principles as those in single-block platforms. However, in this case, the net surface charge arises from the collective contributions of charged groups from the pore wall, enzymes, and the additional constructional block (e.g., polyelectrolytes or MOFs) (Figure 8c). This composite amphoteric arrangement becomes more susceptible to charge state variations due to protonation and deprotonation processes across a wider range of acid-base equilibria, thereby increasing sensitivity to pH changes induced by the generation of acidic or basic reaction products[47,187]. Due to the pH-driven sensing mechanism, special care must be taken when electrostatic self-assembly-based architectures are built, as excess substrate concentrations can generate a sufficient amount of reaction products to induce significant pH shifts within the nanochannel, potentially leading to the detachment and loss of functional elements. This effect is further exacerbated by the continuous flux during measurements [91,104]. As mentioned earlier, the number of building blocks layers can vary

© 2025 by the author(s). Distributed under a Creative Commons CC BY license.

Preprints.org (www.preprints.org) | NOT PEER-REVIEWED | Posted: 2 July 2025 doi:10.20944/preprints202507.0128.v1

among different systems, directly influencing recognition and transduction phenomena. The incorporation of additional recognition element layers has been shown to significantly improve detection limits, sensitivity, and the concentration response range. Additionally, in platforms utilizing enzymatic cascade reactions, the specific enzyme ratio and layer organization play a critical role in optimizing these performance parameters[92]. However, the incorporation of additional layers also impacts on the effective channel size and fabrication complexity. Also, increasing the number of layers can lead to lower recorded currents due to a reduction in channel diameter, and in some cases, complete channel blockage may occur, posing a challenge to system performance and reproducibility[91,104].

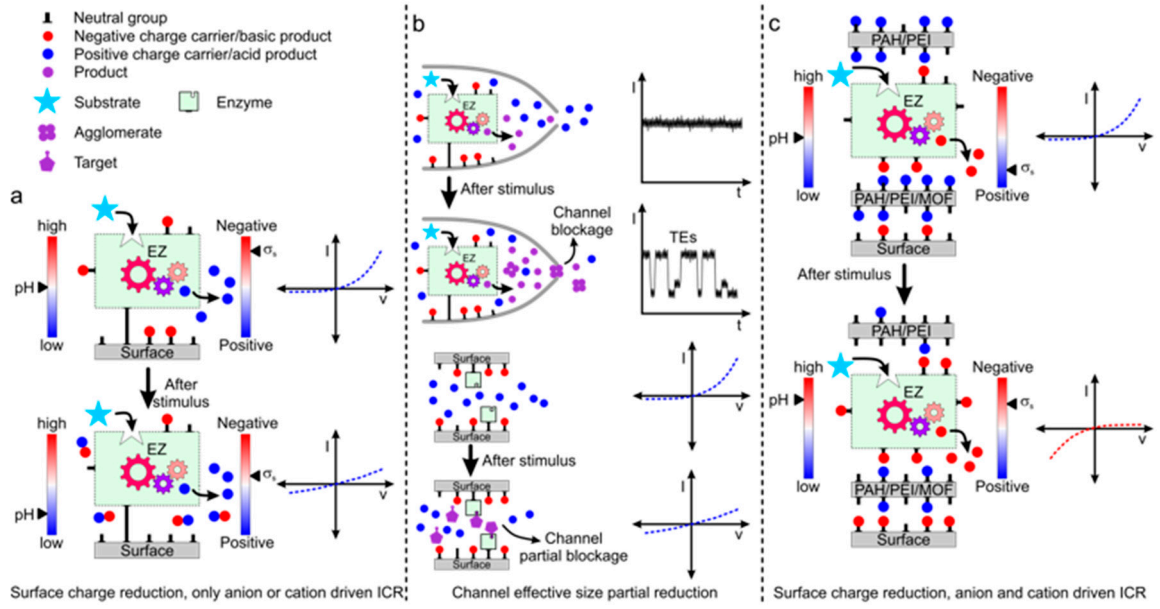

Figure 8. Recognition and transduction mechanisms a) One-block system: The transduction mechanism originates from negative surface charge screening by positive charge carriers. b) One-block system: The transduction mechanism arises from channel obstruction caused by the formation of agglomerates inside the channel or the irreversible binding of large target molecules. c) Two-block system: The transduction mechanism arises from the acid-base equilibrium of the amphoteric groups in the MOF/Polyelectrolyte, the enzyme and the PET surface. Any mechanism may involve concerted enzymatic functions when two or more enzymes are immobilized in the enzyme layer.

From a kinetic perspective, iontronic signals arising from enzyme recognition and transduction mechanisms in single-nanochannel platforms have recently been addressed theoretically by Pérez Sirkin and coworkers[190]. In their study, the influence of kinetic parameters related to enzymatic reactions and the diffusion/migration of substrates and products was analyzed to accurately describe and model experimental results obtained in the one-block system developed by Lin et al[96]. Interestingly, their findings showed that substrate concentration at the channel wall is not a limiting factor. Instead, radial diffusion rapidly equilibrates substrate levels at the surface. In fact, calculations revealed that substrate concentration remains above 60% of the bulk concentration even at the narrowest region of the channel, ensuring its availability for enzyme interaction and continuous reaction. Moreover, when the bulk concentration is much lower than K_M, substrate concentration does not appear to be a limiting factor for system saturation.

It could be expected that reaction products will diffuse rapidly to the center of the channel and exit to the bulk, potentially compromising the detection signal. However, reaction products charged with a charge opposite to that of the channel wall have limited diffusion due to electrostatic interactions with the surface, and this accumulation is the main reason for the surface charge changes, leading to variations in the iontronic output. Nevertheless, excessive accumulation also induces system saturation. For example, the retention of H^+ at the surface results in a localized pH drop, which influences enzyme activity and further affects sensitivity. As a result, larger concentration changes

© 2025 by the author(s). Distributed under a Creative Commons CC BY license.

Preprints.org (www.preprints.org) | NOT PEER-REVIEWED | Posted: 2 July 2025 doi:10.20944/preprints202507.0128.v1

are required to produce a significant iontronic response. Moreover, the neutralization of negatively charged groups occurs more rapidly due to accelerated pH reduction, rendering the channel unresponsive to further substrate additions. This effect is more pronounced in longer nanochannels and in enzymes with higher rate constants (*k*), as extended channel lengths hinder proton diffusion and kinetically favored reactions lead to faster pH changes. Although these findings are based on a one-block system, the development of a two-block system incorporating multilayers revealed that the presence of additional amphoteric groups with varied acid-base equilibria significantly enhances the sensing range before saturation occurs (Table 5).

4. Enzyme-Based SSNs Platforms

Enzyme-modified single-nanochannel sensing systems are highly versatile technologies. As enzymes play fundamental roles in metabolic pathways, enzymatic reaction substrates and products represent a valuable source of information useful in clinical context. For that reason, enzyme integration into a nanochannel-based system, where biochemical processes can be transduced into measurable electrical signals is of great interest. To develop an effective sensing platform by incorporating enzymes into single nanochannels, several key considerations must be addressed, to optimize the stimulus–response mechanism. As discussed earlier, enzymatic reaction products must induce detectable changes in the nanochannel's physical or chemical properties to alter conductance and generate a measurable electrical signal. This effect can occur directly, as in the case of pH variations resulting from the production of acidic or basic species (Table 4), or indirectly, mediated by an intermediary. For instance, some studies have demonstrated how ABTS acts primarily as a charge carrier[105,107]. By interacting with the enzyme and undergoing electron transfer, ABTS becomes ionized and subsequently aggregates. This process alters the electric double layer potential distribution and affects the effective nanochannel size, ultimately influencing the ionic transport and sensor response.

Table 5 summarizes small molecule biomarkers which have been analyzed with enzyme modified nanochannels and some important functional parameters. In general, these systems achieve sub-micromolar detection limits and wide dynamic ranges, which represent a significant advantage—not only due to their ability to detect low-concentration analytes but also because they allow for sample dilution to minimize interferences[91]. A major benefit of these platforms is their simplified measurement setup. In most cases, only voltage control and low-noise current amplification are required, functionalities that are widely available in commercial potentiostats. Furthermore, measurements can be performed under ambient conditions, and the membrane materials used are highly stable and readily accessible. Regarding measurement time, iontronic response changes occur within seconds of substrate exposure. However, full signal stabilization typically takes between 1 to 10 minutes, depending on the specific system and with some exceptions.

Table 5. Single nanochannels enzyme-based biosensors.

Year	target	LOD (μM)	Dynamic ranges (μM)	Response time (min)	Ref
2025	Urea	10	10-10000	≈1	[103]
2025	Adenosine	0.01	0.01-500	4	[104]
2025	Arginine	3	30-3000	5	[92]
2025	Creatinine	0.005	0.005-100	2.5	[91]
2024	Urea	0.0001	0.0001-0.01 and 0.001-1	≈3	[90]
2022	Acetylcholine	0.016	0.001-22.5 and 25-100	≈3	[89]
2018	Urea	0.001	0.001-1	1.5	[88]
2017	H_2O_2	500	500 Qualitative analyses	0.01-1.4	[105]
2014	Glucose	15	15-100	≈10	[96]
2014	Glucose	0.001	0.001-1000	N/F	[99]

© 2025 by the author(s). Distributed under a Creative Commons CC BY license.

Preprints.org (www.preprints.org) | NOT PEER-REVIEWED | Posted: 2 July 2025 doi:10.20944/preprints202507.0128.v1

2011	Concanavalin A	10	10 Qualitative analyses	180	[106]
2011	H_2O_2	0.01	0.01-1	0.8-1.6	[107]

Note 4. Approximated response times are estimated from percentage of response change over time plots if the response time is not specifically defined.

To the best of our knowledge, the work published by Mubarak Ali et al. was the first report of a sensing platform incorporating enzymes into single nanochannel membranes[107]. This system was developed as a sensor for H_2O_2, utilizing the enzymatic reaction that occurs in the presence of immobilized HRP with ABTS as a secondary substrate. In this platform, the sensing signal is generated by the accumulation of $ABTS^{\bullet+}$ at the tip region, leading to a decrease in the recorded current at the high-conductance branch (Figure 9a). This effect arises due to charge screening over the negatively charged surface and steric obstruction of counterion flux. The reaction mechanism involved in the process has been proposed as follows:

$$HRP(Fe^{3+})Porp + H_2O_2 \rightarrow HRP(Fe^{4+}=O)Porp^{\bullet+} + H_2O \quad (1)$$

$$HRP(Fe^{4+}=O)Porp^{\bullet+} + AH \rightarrow HRP(Fe^{4+}=O)Porp + A^{\bullet} \quad (2)$$

$$HRP(Fe^{4+}=O)Porp + AH \rightarrow HRP(Fe^{3+})\ Porp + A^{\bullet} + H_2O \quad (3)$$

Where $HRP(Fe^{n+})Porp$ species represent different oxidation states of peroxidase, while AH and $A^{\bullet}$ correspond to ABTS and $ABTS^{\bullet+}$, respectively. This system exhibited a low detection limit of approximately 10 nM, a reversible response, and the potential for reuse without significant loss of sensing performance. However, the signal-to-noise ratio remained an area for improvement. Following a similar reaction approach, L. Zhu and coworkers reported a few years later another H_2O_2 detection platform[105]. Instead of monitoring the current via CV scans, they focused on translocation events generated by $ABTS^{\bullet+}$ agglomerates inside a nanochannel that was ten times larger (Figure 9c). Due to the increased length and reduced diameter, product accumulation was enhanced, leading to agglomerate formation within the channel and a consequent partial reduction of the effective channel diameter. This work provided a comprehensive analysis of translocation events in such platforms and their dependence on the applied bias; however, further quantitative studies were still required.

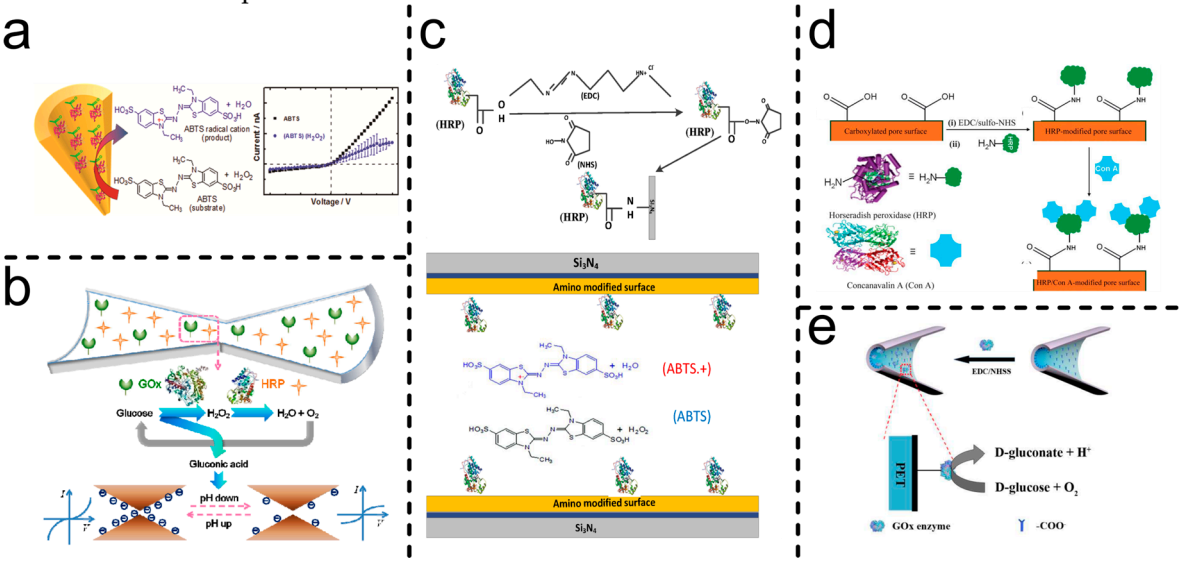

Figure 9. HRP and GOx modified single SSNs by EDC-NHS covalent coupling. a) H_2O_2-responsive nanochannel: The enzymatic reaction produces $ABTS^{\bullet+}$ as a secondary product, whose transport and accumulation induce

© 2025 by the author(s). Distributed under a Creative Commons CC BY license.

Preprints.org (www.preprints.org) | NOT PEER-REVIEWED | Posted: 2 July 2025 doi:10.20944/preprints202507.0128.v1

detectable changes in the recorded current. Adapted with permission from [107] Copyright 2011, American Chemical Society. b) Glucose-responsive nanochannel: The GOx-catalyzed reaction produces H_2O_2 and gluconic acid leading to a decrease in pH and modification of the surface charge, which affects the transmembrane current. HRP facilitates oxygen supply by decomposing H_2O_2 into O_2 and water, sustaining the GOx reaction, Adapted with permission from [96] Copyright 2014, American Chemical Society. c) H_2O_2-responsive nanochannel: The enzymatic reaction produces $ABTS^{\bullet+}$ as a secondary product that accumulates inside the channel and forms agglomerates. The frequency and amplitude of translocation events are related to the applied bias and substrate concentration. Adapted with permission from [105] Copyright 2017, Springer Nature. d) Con A-responsive nanochannel: Con A attachment via glycoprotein–lectin interactions reduces the effective channel size, leading to a decrease in the recorded current Adapted with permission from [106] Copyright 2011, Royal Society Of Chemistry. e) Glucose-responsive nanochannel: Gluconic acid produced by GOx decreases the pH and modifies the recorded current due to surface charge variations. O_2 supply is ensured by saturating the electrolyte before measurement Adapted with permission from [99] Copyright 2014, Royal Society Of Chemistry.

HRP has been used in two additional sensing platforms. A few weeks after the first report by the M. Ali group, they published another work employing this enzyme as a sensing tool for concanavalin A (Con A)[106]. In this case, HRP was covalently immobilized to serve as an anchor point for Con A attachment via glycoprotein–lectin interactions. The study reported that Con A binding led to a reduction in the effective channel diameter and a corresponding decrease in the recorded current in both symmetrical and asymmetrical nanochannels. The findings were further supported by theoretical calculations, which showed good agreement with the experimental results. The authors also highlighted the potential of the platform for quantitative analysis, though additional experiments were required. However, the system is susceptible to interference from monosaccharides such as glucose.

In another study, HRP and GOx were incorporated into a biosensor for glucose detection based on an enzymatic cascade reaction involving the following steps:

$$\text{Glucose} + O_2 + H_2O \rightarrow \text{Gluconic acid} + H_2O_2 \quad (4)$$

$$2H_2O_2 \rightarrow O_2 + 2H_2O \quad (5)$$

In this case, the sensing signal arose from surface charge reduction due to the pH drop caused by the continuous production of gluconic acid. As expected, the O_2 requirement for GOx presents a limitation in aqueous solutions due to the low solubility of O_2 in water. Additionally, H_2O_2 accumulation can lead to GOx degradation. To mitigate both effects, HRP was incorporated to catalyze the subsequent decomposition of H_2O_2 while simultaneously supplying O_2. This approach enabled the first functional device involving concerted enzyme cascade functions within a nanochannel. The system exhibited good switching properties and a short renewal time under cyclical stimulation, demonstrating its potential as a sensing device. Furthermore, it showed good tolerance to galactose, fructose, and mannose, while challenges remained regarding long-term stability and improving the dynamic range[96]. GOx was also employed in another glucose sensing system that similarly relied on pH changes caused by gluconic acid production[99], as shown in reaction 4. However, since this platform lacked HRP, the measurement electrolyte solution was pre-saturated with O_2 to ensure an adequate supply for the reaction. The system demonstrated a low detection limit (~1 nM) and a wider dynamic range (Table 5). Additionally, the influence of channel size on sensing performance was analyzed across a broad range of tip diameters. The modified nanochannel was also exposed to L-glucose and D-glucose, showing high specificity for dextrose and good reversibility in experiments with alternating substrate exposure. However, further studies on response time and storage stability are required to advance toward full device integration.

Urease and acetylcholinesterase have been also integrated into single nanochannel systems for urea and acetylcholine sensing. Unlike the previously mentioned one-block platforms, these systems incorporate an additional functional block to enhance performance. The first approach to urea biosensing was reported by Pérez-Mitta and coworkers[88]. In this work poly(allylamine) was

© 2025 by the author(s). Distributed under a Creative Commons CC BY license.

Preprints.org (www.preprints.org) | NOT PEER-REVIEWED | Posted: 2 July 2025 doi:10.20944/preprints202507.0128.v1

electrostatically assembled onto the anionic pore walls, followed by the electrostatic immobilization of urease. This design enabled rapid and highly sensitive urea detection, with the weak polyelectrolyte acting as a 'reactive signal amplifier' by enhancing the pH changes induced by the enzymatic reaction (Reaction 6). A similar platform was later developed for acetylcholine sensing, employing polyethyleneimine as the secondary functional block[89]. While sharing similar functional principles, this system differed in that the enzymatic reaction led to a decrease in pH due to the production of acetic acid, as shown in Reaction 7.

$$\text{Urea} + 3H_2O \rightarrow 2NH_4^+ + HCO_3^- + OH^- \quad (6)$$

$$\text{Acetylcholine} \rightarrow \text{Choline} + CH_3COO^- + H^+ \quad (7)$$

The presence of additional charged groups with different acid-base equilibria resulted in a broad dynamic pH operational range, allowing signal detection in both anion- and cation-driven ion current rectification states. These platforms not only introduced a novel approach for urea and acetylcholine determination but also laid the foundation for the development of single nanochannel biosensors incorporating additional functional elements to enhance sensing performance. In subsequent years, additional urease-based platforms employing a two-block architecture have been reported, utilizing the same pH-dependent sensing mechanism described in reaction (6) but with improved performance. For instance, building on previous studies of nanoprecipitation phenomena in nanochannels with broken symmetry in the presence of polyvalent or asymmetric electrolytes [137,191] the PAH/Urease system was applied to urea detection in KCl electrolyte solutions containing divalent salts ($MgCl_2$, $CaCl_2$)[90]. A significant enhancement in sensitivity was observed, achieving sub-nanomolar detection limits. In summary, the enzymatic reaction increases the pH inside the nanochannel, leading to an increase in negative surface charge. This, in turn, promotes nanoprecipitation, which functions as a reactive signal amplification mechanism, enabling lower detection limits compared to previous systems. Additionally, in a more recent study[103], Huamani et al. developed a stability-enhanced urea sensing platform by employing a covalently attached UiO-66-NH_2-Urease arrangement instead of the electrostatically immobilized PAH/Urease system. This new configuration not only retained its functional sensing capabilities but also exhibited greater stability under various measurement conditions, alternating substrate exposures, and continuous flow experiments, challenges that remain significant in electrostatically immobilized enzyme platforms.

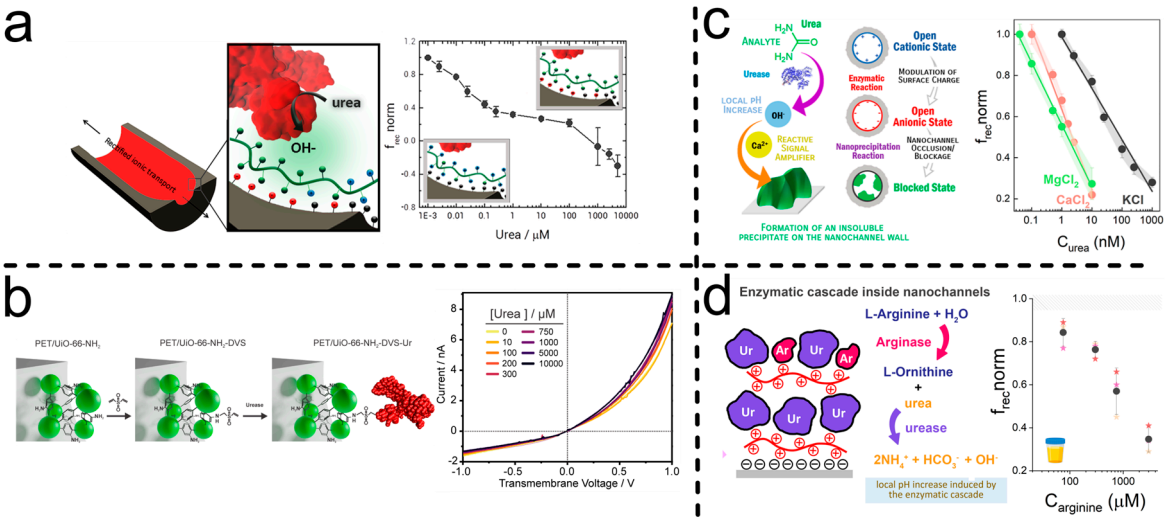

Figure 10. Urease- and arginase-modified single SSNs were prepared via electrostatic self-assembly or MOF-DVS cross-linking. a) Adapted with permission from [88] Copyright 2018, American Chemical Society, b) [103] and c) Adapted with permission from [90] Copyright 2024, American Chemical Society. Represent urease-responsive nanochannels, where current and ICR are influenced by surface charge changes due to the pH

© 2025 by the author(s). Distributed under a Creative Commons CC BY license.

Preprints.org (www.preprints.org) | NOT PEER-REVIEWED | Posted: 2 July 2025 doi:10.20944/preprints202507.0128.v1

increase caused by NH_3 production. d) Arginine-responsive nanochannel: Arginase catalyzes the conversion of arginine into urea, which is subsequently decomposed by urease. The resulting NH_3 production increases the pH, leading to surface charge modifications and changes in ICR, Adapted with permission from [92] Copyright 2025, Royal Society Of Chemistry.

Following the concept of concerted functions arising from cascade enzymatic reactions, a new strategy for arginine biosensing based on a multilayer architecture incorporating urease and arginase via electrostatic self-assembly, with PAH serving as the positively charged block has been recently reported[92]. Arginine detection is achieved through a sequential catalytic process, where arginine is firstly converted into urea by arginase (Reaction 8), and urea is subsequently hydrolyzed by urease to produce ammonia, leading to a local pH increase (Reaction 6).

$$\text{L-Arginine} + H_2O \rightarrow \text{L-Ornithine} + \text{Urea} \quad (8)$$

Beyond demonstrating effective arginine detection with high selectivity against non-target amino acids, this platform also enabled a detailed investigation of key design parameters. Specifically, the number of layers, their organization, and the composition ratio significantly influenced the detection limits and dynamic range. Moreover, along with the creatinine and adenosine biosensors[91,104], this system is among the few enzyme-based single SSNs biosensors that have been tested in complex real samples, assessing their performance in complex biological matrices. The creatinine biosensing platform was developed by integrating creatinine deaminase and polyethyleneimine in a multilayer "sandwich" configuration, as illustrated in Figure 7d. Notably, the incorporation of an additional polyelectrolyte layer over the enzyme significantly enhanced structural stability and expanded the functional dynamic range compared to the simpler bilayer arrangement (Figure 7c). The sensing mechanism is based on charge variations induced by local pH changes, as creatinine undergoes enzymatic deamination, producing ammonia through the following reaction:

$$\text{Creatinine} + H_2O \rightarrow \text{N-methylhydantoin} + NH_4^+ + OH^- \quad (9)$$

Special consideration must be given to electrostatically assembled multilayer architectures, as strong pH variations can weaken interactions between charged layers, potentially leading to block detachment and enzyme loss, ultimately affecting device performance. This phenomenon was also observed in a recent work, where adenosine deaminase was immobilized in a similar sandwich-type architecture using polyallylamine[104]. The functional principle remained the same: adenosine deaminase catalyses the deamination of adenosine, generating ammonia and inosine (Reaction 10).

$$\text{Adenosine} + H_2O \rightarrow \text{Inosine} + NH_4^+ + OH^- \quad (10)$$

For both sandwich-structured biosensors, interference, response time, and storage stability studies were carried out. In general, the response time was short (<5 min), and good selectivity was achieved when testing common metabolites found in real samples. However, sensor performance was significantly affected by phosphate-containing species and high concentrations of proteins such as BSA, likely due to their irreversible adsorption onto the positively charged polyelectrolyte surface. Regarding storage stability, dry conditions and low temperatures (~4°C) helped preserve sensor functionality in the medium term, though a gradual loss of response capability was observed over time.

© 2025 by the author(s). Distributed under a Creative Commons CC BY license.

Preprints.org (www.preprints.org) | NOT PEER-REVIEWED | Posted: 2 July 2025 doi:10.20944/preprints202507.0128.v1

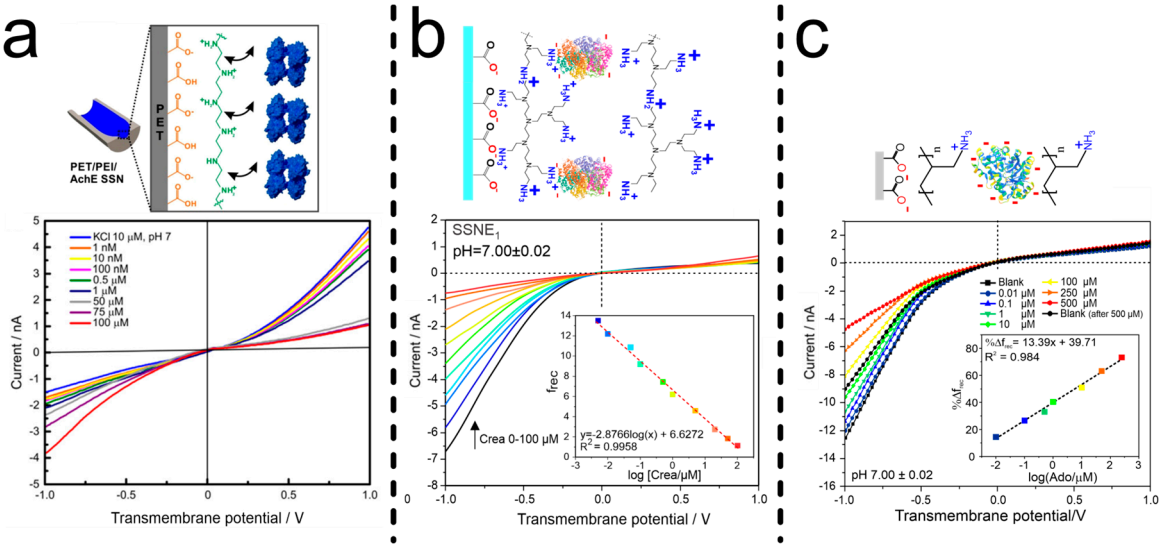

Figure 11. Electrostatic self-assembly-modified single SSNs: Enzymatic reactions induce surface charge variations through OH^- or H^+ production, leading to changes in ionic current rectification (ICR) depending on substrate concentration. a) Acetylcholine-, b) Creatinine-, and c) Adenosine-responsive nanochannels. Adapted with permission from a) [89] Copyright 2022, Royal Society Of Chemistry, b) [91] Copyright 2025, Royal Society Of Chemistry and c) [104].

5. Challenges: Toward Future Developments

Despite demonstrating excellent functionality features, these sensing platforms still face major challenges for future clinical applications. One of the most pressing concerns is system stability over time. Storage stability studies have only recently been explored and remain superficially addressed[91,104]. Initial results indicate a decline in performance after short storage periods. Additionally, as nanofluidic devices, these sensors require further research into continuous substrate measurement to facilitate real-time biomarker monitoring. In this context, continuous and unidirectional flow measurements are essential to assess long-term response stability and device durability. Another critical factor is tolerance to biological sample interferences. Although enzymatic selectivity ensures high specificity for the target substrate, systems based on polyelectrolytes are susceptible to divalent anion interactions and protein adsorption. Specifically, amino-phosphate interactions [192–194] and negatively charged proteins can significantly affect performance in real sample applications, necessitating sample pretreatment in current designs.

A promising approach to enhanced interference tolerance and expanding stimulus–response mechanisms is the incorporation of additional functional structural components. For example, recent applications of metal-organic frameworks have demonstrated improved system stability. Moreover, various enzyme immobilization strategies remain unexplored in nanochannel-based sensors and could further enhance performance. The potential of enzyme-based sensing systems for continuous health monitoring is evident. Platforms currently used in continuous glucose monitoring devices have demonstrated that enzyme-based sensors can function as daily monitoring tools. Although it took decades for enzyme electrodes to evolve into widely used medical devices, they now provide millions of people with greater independence and improved healthcare management. While nanofluidic sensing technologies are still in their early stages, they are continuously advancing, and their potential continues to grow. With further development, these systems could become reliable analytical tools for clinical diagnostics and real-time biomarker analysis.

Acknowledgments: LMH-P acknowledges a scholarship from CONICET. OA and WAM are CONICET staff members. The authors acknowledge the financial support from Universidad Nacional de La Plata (PPID-X1016) and ANPCyT (PICT-2020-SERIEA-02468).

© 2025 by the author(s). Distributed under a Creative Commons CC BY license.

Preprints.org (www.preprints.org) | NOT PEER-REVIEWED | Posted: 2 July 2025 doi:10.20944/preprints202507.0128.v1

Abbreviations and Symbols

The following abbreviations and symbols are used in this manuscript:

PET	Polyethylene terephthalate
PC	Polycarbonate
PP	Polypropylene
PVDF	Polyvinylidene fluoride
CR39	Poly (allyl diglycol carbonate)
f_{rec}	Rectification factor
TEs	Translocation events
PNP	Poisson–Nernst–Planck
ICR	Ion current rectification
PI	Polyimide
PBD	Protein data bank
SSNs	Solid state nanochannels
EBL	Electron beam lithography
RIE	Reactive ion etching
FIB	Focused ion beam
IBS	Ion beam sculping
EE-PEO	Embedding electrospun polyethylene oxide
EB	Electron bean
LMIS	Liquid metal ion source
PFA	Perfluoroalkyl passivation
EDC	1-Ethyl-3-(3-dimethylaminopropyl) carbodiimide
NHS	N-Hydroxy succinimide
MOF	Metal organic framework
DVS	Divinyl sulfone
PAH	Poly (allylamine Hydrochloride)
PEI	Polyethyleneimine
EZ	Enzyme
GOx	Glucose oxidase
ADA	Adenosine deaminase
CD	Creatinine deaminase
AchE	Acetyl cholinesterase
HRP	Horseradish peroxidase
PLL	Poly-L-Lysine
Con A	Concanavalin A
CV	Cyclic voltammetry
SEM	Scanning electron microscopy
TEM	Transmission electron microscopy
LP-CVD	Low pressure chemical vapor deposition
EDL	Electrical double layer

© 2025 by the author(s). Distributed under a Creative Commons CC BY license.

Preprints.org (www.preprints.org) | NOT PEER-REVIEWED | Posted: 2 July 2025 doi:10.20944/preprints202507.0128.v1

σ_s	Surface charge density
F	Faraday constant
R	Gas constant
Γ_i	Surface density
q_i	Net charge
z_i	Valence of ion
e	Electron charge
ψ	Electric potential
ε_0	Vacuum permittivity
ε_r	Relative permittivity
k_B	Boltzmann constant
x	Spatial coordinate
T	Absolute temperature
n_i^{∞}	Bulk volume density
n	Volume density
λ_D	Debye length
κ	Debye-Hückel parameter
I_s	Ionic strength
G	Conductance
μ	Mobility
u	Fluid velocity
l	Length
r	Radial coordinate
I	Current
V	Potential
D_i	Diffusion coefficient
J_i	Flux per area
Φ	Electric potential
c_i	Concentration
ρ	Density
η	Viscosity
p	Pressure

References

1. Atkinson, A.J.; Colburn, W.A.; DeGruttola, V.G.; DeMets, D.L.; Downing, G.J.; Hoth, D.F.; Oates, J.A.; Peck, C.C.; Schooley, R.T.; Spilker, B.A.; et al. Biomarkers and Surrogate Endpoints: Preferred Definitions and Conceptual Framework. *Clin Pharmacol Ther* **2001**, *69*, 89–95, doi:10.1067/mcp.2001.113989.
2. Demirci-Çekiç, S.; Özkan, G.; Avan, A.N.; Uzunboy, S.; Çapanoğlu, E.; Apak, R. Biomarkers of Oxidative Stress and Antioxidant Defense. *J Pharm Biomed Anal* **2022**, *209*, 114477, doi:10.1016/j.jpba.2021.114477.
3. Hansson, O. Biomarkers for Neurodegenerative Diseases. *Nature Medicine 2021 27:6* **2021**, *27*, 954–963, doi:10.1038/s41591-021-01382-x.
4. Brucker, N.; do Nascimento, S.N.; Bernardini, L.; Charão, M.F.; Garcia, S.C. Biomarkers of Exposure, Effect, and Susceptibility in Occupational Exposure to Traffic-Related Air Pollution: A Review. *Journal of Applied Toxicology* **2020**, *40*, 722–736, doi:10.1002/jat.3940.

© 2025 by the author(s). Distributed under a Creative Commons CC BY license.

Preprints.org (www.preprints.org) | NOT PEER-REVIEWED | Posted: 2 July 2025 doi:10.20944/preprints202507.0128.v1

5. Alaimo, A.; Vaira, V.; Sarhadi, V.K.; Armengol, G. Molecular Biomarkers in Cancer. *Biomolecules 2022, Vol. 12, Page 1021* **2022**, *12*, 1021, doi:10.3390/biom12081021.
6. Karaboğa, M.N.S.; Sezgintürk, M.K. Biosensor Approaches on the Diagnosis of Neurodegenerative Diseases: Sensing the Past to the Future. *J Pharm Biomed Anal* **2022**, *209*, 114479, doi:10.1016/j.jpba.2021.114479.
7. Xing, G.; Ai, J.; Wang, N.; Pu, Q. Recent Progress of Smartphone-Assisted Microfluidic Sensors for Point of Care Testing. *TrAC Trends in Analytical Chemistry* **2022**, *157*, 116792, doi:10.1016/j.trac.2022.116792.
8. Wang, C.; He, T.; Zhou, H.; Zhang, Z.; Lee, C. Artificial Intelligence Enhanced Sensors - Enabling Technologies to next-Generation Healthcare and Biomedical Platform. *Bioelectron Med* **2023**, *9*, 17, doi:10.1186/s42234-023-00118-1.
9. Park, J.; Seo, B.; Jeong, Y.; Park, I. A Review of Recent Advancements in Sensor-Integrated Medical Tools. *Advanced Science* **2024**, *11*, 2307427, doi:10.1002/advs.202307427.
10. Zheng, L.; Cao, M.; Du, Y.; Liu, Q.; Emran, M.Y.; Kotb, A.; Sun, M.; Ma, C.-B.; Zhou, M. Artificial Enzyme Innovations in Electrochemical Devices: Advancing Wearable and Portable Sensing Technologies. *Nanoscale* **2024**, *16*, 44–60, doi:10.1039/D3NR05728C.
11. Kaur, A.; Rohilla, R.; Rana, S.; Rani, S.; Prabhakar, N. Recent Advances in Protein Biomarkers Based Enzymatic Biosensors for Non-Communicable Diseases. *TrAC Trends in Analytical Chemistry* **2024**, *174*, 117683, doi:10.1016/j.trac.2024.117683.
12. Xiao, X.; Ulstrup, J. Towards Continuous Potentiometric Enzymatic Biosensors. *Curr Opin Electrochem* **2024**, *46*, 101549, doi:10.1016/j.coelec.2024.101549.
13. Lino, C.; Barrias, S.; Chaves, R.; Adega, F.; Martins-Lopes, P.; Fernandes, J.R. Biosensors as Diagnostic Tools in Clinical Applications. *Biochimica et Biophysica Acta (BBA) - Reviews on Cancer* **2022**, *1877*, 188726, doi:10.1016/j.bbcan.2022.188726.
14. Williams, A.; Aguilar, M.R.; Pattiya Arachchillage, K.G.G.; Chandra, S.; Rangan, S.; Ghosal Gupta, S.; Artes Vivancos, J.M. Biosensors for Public Health and Environmental Monitoring: The Case for Sustainable Biosensing. *ACS Sustain Chem Eng* **2024**, *12*, 10296–10312, doi:10.1021/acssuschemeng.3c06112.
15. Liu, W.; Chung, K.; Yu, S.; Lee, L.P. Nanoplasmonic Biosensors for Environmental Sustainability and Human Health. *Chem Soc Rev* **2024**, *53*, 10491–10522, doi:10.1039/D3CS00941f.
16. Heckmann, C.M.; Paradisi, F. Looking Back: A Short History of the Discovery of Enzymes and How They Became Powerful Chemical Tools. *ChemCatChem* **2020**, *12*, 6082–6102, doi:10.1002/cctc.202001107.
17. Tamanoi, F. History of The Enzymes: 1950–2023. In *The Enzymes*; Academic Press, 2023; Vol. 54, pp. 3–11 ISBN 9780443136917.
18. Colin J. Suckling *Enzyme Chemistry*; Suckling, C.J., Ed.; Springer Netherlands: Dordrecht, 1990; ISBN 978-94-010-7317-2.
19. Clark Jr, L.C.; Lyons, C. Annals. *New York Academy of Sciences* **1962**, *102*, 29–145, doi:10.1111/j.1749-6632.1962.tb13623.x.
20. Updike, S.J.; Hicks, G.P. The Enzyme Electrode. *Nature 1967 214:5092* **1967**, *214*, 986–988, doi:10.1038/214986a0.
21. Cavalcante, F.T.T.; de A. Falcão, I.R.; da S. Souza, J.E.; Rocha, T.G.; de Sousa, I.G.; Cavalcante, A.L.G.; de Oliveira, A.L.B.; de Sousa, M.C.M.; dos Santos, J.C.S. Designing of Nanomaterials-Based Enzymatic Biosensors: Synthesis, Properties, and Applications. *Electrochem* **2021**, *2*, 149–184, doi:10.3390/electrochem2010012.
22. Maghraby, Y.R.; El-Shabasy, R.M.; Ibrahim, A.H.; Azzazy, H.M.E.-S. Enzyme Immobilization Technologies and Industrial Applications. *ACS Omega* **2023**, *8*, 5184–5196, doi:10.1021/acsomega.2c07560.
23. MacKinnon, R. Potassium Channels and the Atomic Basis of Selective Ion Conduction (Nobel Lecture). *Angewandte Chemie International Edition* **2004**, *43*, 4265–4277, doi:10.1002/anie.200400662.
24. Agre, P. Aquaporin Water Channels. *Biosci Rep* **2004**, *24*, 127–163, doi:10.1007/s10540-005-2577-2.
25. Scrimin, P.; Tecilla, P. Model Membranes: Developments in Functional Micelles and Vesicles. *Curr Opin Chem Biol* **1999**, *3*, 730–735, doi:10.1016/S1367-5931(99)90031-5.
26. Matile, S.; Som, A.; Sordé, N. Recent Synthetic Ion Channels and Pores. *Tetrahedron* **2004**, *60*, 6405–6435, doi:10.1016/j.tet.2004.05.052.

© 2025 by the author(s). Distributed under a Creative Commons CC BY license.

Preprints.org (www.preprints.org) | NOT PEER-REVIEWED | Posted: 2 July 2025 doi:10.20944/preprints202507.0128.v1

27. Gokel, G.W.; Mukhopadhyay, A. Synthetic Models of Cation-Conducting Channels. *Chem Soc Rev* **2001**, *30*, 274–286, doi:10.1039/b008667n.
28. Siwy, Z.; Apel, P.; Baur, D.; Dobrev, D.D.; Korchev, Y.E.; Neumann, R.; Spohr, R.; Trautmann, C.; Voss, K.O. Preparation of Synthetic Nanopores with Transport Properties Analogous to Biological Channels. *Surf Sci* **2003**, *532–535*, 1061–1066, doi:10.1016/S0039-6028(03)00448-5.
29. Ma, T.; Janot, J.; Balme, S. Track-Etched Nanopore/Membrane: From Fundamental to Applications. *Small Methods* **2020**, *4*, 2000366, doi:10.1002/smtd.202000366.
30. Kaya, D.; Keçeci, K. Review—Track-Etched Nanoporous Polymer Membranes as Sensors: A Review. *J Electrochem Soc* **2020**, *167*, 037543, doi:10.1149/1945-7111/ab67a7.
31. Zeng, J.; Schmitz, F.; Isaksson, S.; Glas, J.; Arbab, O.; Andersson, M.; Sundell, K.; Eriksson, L.A.; Swaminathan, K.; Törnroth-Horsefield, S.; et al. High-Resolution Structure of a Fish Aquaporin Reveals a Novel Extracellular Fold. *Life Sci Alliance* **2022**, *5*, e202201491, doi:10.26508/lsa.202201491.
32. Zuniga, D.; Zoumpoulakis, A.; Veloso, R.F.; Peverini, L.; Shi, S.; Pozza, A.; Kugler, V.; Bonneté, F.; Bouceba, T.; Wagner, R.; et al. Biochemical, Biophysical, and Structural Investigations of Two Mutants (<scp>C154Y</Scp> and <scp>R312H</Scp>) of the Human Kir2.1 Channel Involved in the Andersen-Tawil Syndrome. *The FASEB Journal* **2024**, *38*, e70146, doi:10.1096/fj.202401567R.
33. Stoikov, I.I.; Antipin, I.S.; Konovalov, A.I. Artificial Ion Channels. *Russian Chemical Reviews* **2003**, *72*, 1055–1077, doi:10.1070/RC2003v072n12ABEH000834.
34. Kan, X.; Wu, C.; Wen, L.; Jiang, L. Biomimetic Nanochannels: From Fabrication Principles to Theoretical Insights. *Small Methods* **2022**, *6*, 2101255, doi:10.1002/smtd.202101255.
35. Steinbacher, S.; Bass, R.; Strop, P.; Rees, D.C. Structures of the Prokaryotic Mechanosensitive Channels MscL and MscS. In *Current Topics in Membranes*; Academic Press, 2007; Vol. 58, pp. 1–24 ISBN 0121533581.
36. Tanaka, Y.; Hirano, N.; Kaneko, J.; Kamio, Y.; Yao, M.; Tanaka, I. 2-Methyl-2,4-pentanediol Induces Spontaneous Assembly of Staphylococcal A-hemolysin into Heptameric Pore Structure. *Protein Science* **2011**, *20*, 448–456, doi:10.1002/pro.579.
37. Tanaka, K.; Caaveiro, J.M.M.; Morante, K.; González-Manãs, J.M.; Tsumoto, K. Structural Basis for Self-Assembly of a Cytolytic Pore Lined by Protein and Lipid. *Nature Communications 2015 6:1* **2015**, *6*, 1–11, doi:10.1038/ncomms7337.
38. Wang, S.; Zhao, Z.; Haque, F.; Guo, P. Engineering of Protein Nanopores for Sequencing, Chemical or Protein Sensing and Disease Diagnosis. *Curr Opin Biotechnol* **2018**, *51*, 80–89, doi:10.1016/j.copbio.2017.11.006.
39. Peng, W.; de Souza Santos, M.; Li, Y.; Tomchick, D.R.; Orth, K. High-Resolution Cryo-EM Structures of the E. Coli Hemolysin ClyA Oligomers. *PLoS One* **2019**, *14*, e0213423, doi:10.1371/journal.pone.0213423.
40. Grahame, D.A.S.; Bryksa, B.C.; Yada, R.Y. Factors Affecting Enzyme Activity. In *Improving and Tailoring Enzymes for Food Quality and Functionality*; Elsevier, 2015; pp. 11–55 ISBN 9781782422976.
41. Feng, Y.; Xu, Y.; Liu, S.; Wu, D.; Su, Z.; Chen, G.; Liu, J.; Li, G. Recent Advances in Enzyme Immobilization Based on Novel Porous Framework Materials and Its Applications in Biosensing. *Coord Chem Rev* **2022**, *459*, 214414, doi:10.1016/j.ccr.2022.214414.
42. Bolivar, J.M.; Woodley, J.M.; Fernandez-Lafuente, R. Is Enzyme Immobilization a Mature Discipline? Some Critical Considerations to Capitalize on the Benefits of Immobilization. *Chem Soc Rev* **2022**, *51*, 6251–6290, doi:10.1039/D2CS00083K.
43. Huang, Y.; Liu, L.; Luo, C.; Liu, W.; Lou, X.; Jiang, L.; Xia, F. Solid-State Nanochannels for Bio-Marker Analysis. *Chem Soc Rev* **2023**, *52*, 6270–6293, doi:10.1039/D2CS00865C.
44. Laucirica, G.; Toum Terrones, Y.; Cayón, V.; Cortez, M.L.; Toimil-Molares, M.E.; Trautmann, C.; Marmisollé, W.; Azzaroni, O. Biomimetic Solid-State Nanochannels for Chemical and Biological Sensing Applications. *TrAC Trends in Analytical Chemistry* **2021**, *144*, 116425, doi:10.1016/j.trac.2021.116425.
45. Li, X.; Zhu, C.; Wu, Y.; Kong, X.-Y.; Wen, L. Bioinspired Solid-State Nanochannels for Molecular Analysis. *Nanoscale* **2025**, *17*, 1225–1237, doi:10.1039/D4NR03711A.
46. Jiang, X.; Wang, L.; Liu, S.; Li, F.; Liu, J. Bioinspired Artificial Nanochannels: Construction and Application. *Mater Chem Front* **2021**, *5*, 1610–1631, doi:10.1039/D0QM00795A.

© 2025 by the author(s). Distributed under a Creative Commons CC BY license.

Preprints.org (www.preprints.org) | NOT PEER-REVIEWED | Posted: 2 July 2025 doi:10.20944/preprints202507.0128.v1

47. Ding, D.; Gao, P.; Ma, Q.; Wang, D.; Xia, F. Biomolecule-Functionalized Solid-State Ion Nanochannels/Nanopores: Features and Techniques. *Small* **2019**, *15*, 1804878, doi:10.1002/smll.201804878.
48. Ma, Q.; Si, Z.; Li, Y.; Wang, D.; Wu, X.; Gao, P.; Xia, F. Functional Solid-State Nanochannels for Biochemical Sensing. *TrAC Trends in Analytical Chemistry* **2019**, *115*, 174–186, doi:10.1016/j.trac.2019.04.014.
49. Kuanaeva, R.M.; Vaneev, A.N.; Gorelkin, P. V.; Erofeev, A.S. Nanopipettes as a Potential Diagnostic Tool for Selective Nanopore Detection of Biomolecules. *Biosensors (Basel)* **2024**, *14*, 627, doi:10.3390/bios14120627.
50. Ma, H.; Yu, R.-J.; Ying, Y.-L.; Long, Y.-T. Electrochemically Confined Effects on Single Enzyme Detection with Nanopipettes. *Journal of Electroanalytical Chemistry* **2022**, *908*, 116086, doi:10.1016/j.jelechem.2022.116086.
51. Bulbul, G.; Chaves, G.; Olivier, J.; Ozel, R.E.; Pourmand, N. Nanopipettes as Monitoring Probes for the Single Living Cell: State of the Art and Future Directions in Molecular Biology. *Cells* **2018**, *7*, 55, doi:10.3390/cells7060055.
52. Wang, H.; Tang, H.; Qiu, X.; Li, Y. Solid-State Glass Nanopipettes: Functionalization and Applications. *Chemistry – A European Journal* **2024**, *30*, e202400281, doi:10.1002/chem.202400281.
53. Zheng, S.; Wu, M.; Wang, X.; Xu, S.; Qian, R. Nanopipettes for Chemical Analysis in Life Sciences. *ChemBioChem* **2025**, *26*, e202400879, doi:10.1002/cbic.202400879.
54. Stanley, J.; Pourmand, N. Nanopipettes—The Past and the Present. *APL Mater* **2020**, *8*, doi:10.1063/5.0020011.
55. Zhang, Y.; Reisner, W. Fabrication and Characterization of Nanopore-Interfaced Nanochannel Devices. *Nanotechnology* **2015**, *26*, 455301, doi:10.1088/0957-4484/26/45/455301.
56. Li, J.; Stein, D.; McMullan, C.; Branton, D.; Aziz, M.J.; Golovchenko, J.A. Ion-Beam Sculpting at Nanometre Length Scales. *Nature* **2001**, *412*, 166–169, doi:10.1038/35084037.
57. Lo, C.J.; Aref, T.; Bezryadin, A. Fabrication of Symmetric Sub-5 Nm Nanopores Using Focused Ion and Electron Beams. *Nanotechnology* **2006**, *17*, 3264–3267, doi:10.1088/0957-4484/17/13/031.
58. Fürjes, P. Controlled Focused Ion Beam Milling of Composite Solid State Nanopore Arrays for Molecule Sensing. *Micromachines (Basel)* **2019**, *10*, 774, doi:10.3390/mi10110774.
59. Zhou, L.; Chen, Z.; Ma, J. A Simple Cost-Effective Method to Fabricate Single Nanochannels by Embedding Electrospun Polyethylene Oxide Nanofibers. *ChemistryOpen* **2024**, *13*, e202400008, doi:10.1002/open.202400008.
60. Zhang, B.; Galusha, J.; Shiozawa, P.G.; Wang, G.; Bergren, A.J.; Jones, R.M.; White, R.J.; Ervin, E.N.; Cauley, C.C.; White, H.S. Bench-Top Method for Fabricating Glass-Sealed Nanodisk Electrodes, Glass Nanopore Electrodes, and Glass Nanopore Membranes of Controlled Size. *Anal Chem* **2007**, *79*, 4778–4787, doi:10.1021/ac070609j.
61. Ling, Y.; Yang, X.; Zhou, L.; Lei, Z.; Hou, Y.; Hou, X. Current Progress in Glass-Based Nanochannels. *Int J Smart Nano Mater* **2024**, *15*, 222–237, doi:10.1080/19475411.2024.2305544.
62. Sha, J.; Ni, Z.; Liu, L.; Yi, H.; Chen, Y. A Novel Method of Fabricating a Nanopore Based on a Glass Tube for Single-Molecule Detection. *Nanotechnology* **2011**, *22*, 175304, doi:10.1088/0957-4484/22/17/175304.
63. Kamai, H.; Xu, Y. Fabrication of Ultranarrow Nanochannels with Ultrasmall Nanocomponents in Glass Substrates. *Micromachines (Basel)* **2021**, *12*, 775, doi:10.3390/mi12070775.
64. Li, N.; Yu, S.; Harrell, C.C.; Martin, C.R. Conical Nanopore Membranes. Preparation and Transport Properties. *Anal Chem* **2004**, *76*, 2025–2030, doi:10.1021/ac035402e.
65. Liu, F.; Wang, M.; Wang, X.; Wang, P.; Shen, W.; Ding, S.; Wang, Y. Fabrication and Application of Nanoporous Polymer Ion-Track Membranes. *Nanotechnology* **2019**, *30*, 052001, doi:10.1088/1361-6528/aaed6d.
66. Apel, P.Y.; Blonskaya, I. V.; Dmitriev, S.N.; Orelovitch, O.L.; Presz, A.; Sartowska, B.A. Fabrication of Nanopores in Polymer Foils with Surfactant-Controlled Longitudinal Profiles. *Nanotechnology* **2007**, *18*, 305302, doi:10.1088/0957-4484/18/30/305302.
67. Cornelius, T.W.; Apel, P.Yu.; Schiedt, B.; Trautmann, C.; Toimil-Molares, M.E.; Karim, S.; Neumann, R. Investigation of Nanopore Evolution in Ion Track-Etched Polycarbonate Membranes. *Nucl Instrum Methods Phys Res B* **2007**, *265*, 553–557, doi:10.1016/j.nimb.2007.10.004.

© 2025 by the author(s). Distributed under a Creative Commons CC BY license.

Preprints.org (www.preprints.org) | NOT PEER-REVIEWED | Posted: 2 July 2025 doi:10.20944/preprints202507.0128.v1

68. Fink, D.; Hnatowicz, V. Transport Processes in Low-Energy Ion-Irradiated Polymers. In; Springer, Berlin, Heidelberg, 2004; pp. 47–91 ISBN 978-3-662-10608-2.
69. Wang, P.; Laskin, J. *Ion Beams in Nanoscience and Technology*; Hellborg, R., Whitlow, H.J., Zhang, Y., Eds.; Particle Acceleration and Detection; Springer Berlin Heidelberg: Berlin, Heidelberg, 2010; ISBN 978-3-642-00622-7.
70. Apel, P. Track Etching Technique in Membrane Technology. *Radiat Meas* **2001**, *34*, 559–566, doi:10.1016/S1350-4487(01)00228-1.
71. Apel, P.Y.; Blonskaya, I. V.; Lizunov, N.E.; Olejniczak, K.; Orelovitch, O.L.; Sartowska, B.A.; Dmitriev, S.N. Asymmetrical Nanopores in Track Membranes: Fabrication, the Effect of Nanopore Shape and Electric Charge of Pore Walls, Promising Applications. *Russian Journal of Electrochemistry* **2017**, *53*, 58–69, doi:10.1134/S1023193517010037.
72. Apel, P.Y.; Blonskaya, I.V.; Didyk, A.Y.; Dmitriev, S.N.; Orelovitch, O.L.; Root, D.; Samoilova, L.I.; Vutsadakis, V.A. Surfactant-Enhanced Control of Track-Etch Pore Morphology. *Nucl Instrum Methods Phys Res B* **2001**, *179*, 55–62, doi:10.1016/S0168-583X(00)00691-1.
73. Trautmann, C.; Brüchle, W.; Spohr, R.; Vetter, J.; Angert, N. Pore Geometry of Etched Ion Tracks in Polyimide. *Nucl Instrum Methods Phys Res B* **1996**, *111*, 70–74, doi:10.1016/0168-583X(95)01264-8.
74. Vlassiouk, I.; Apel, P.Y.; Dmitriev, S.N.; Healy, K.; Siwy, Z.S. Versatile Ultrathin Nanoporous Silicon Nitride Membranes. *Proceedings of the National Academy of Sciences* **2009**, *106*, 21039–21044, doi:10.1073/pnas.0911450106.
75. Toum Terrones, Y.; Laucirica, G.; Cayón, V.M.; Cortez, M.L.; Toimil-Molares, M.E.; Trautmann, C.; Marmisollé, W.A.; Azzaroni, O. Ionic Nanoarchitectonics for Nanochannel-Based Biosensing Devices. In *Materials Nanoarchitectonics*; Elsevier, 2024; pp. 429–452 ISBN 9780323994729.
76. Bodansky, D. *Nuclear Energy*; Springer New York: New York, NY, 2005; ISBN 978-0-387-20778-0.
77. Basu, D.; Miroshnik, V.W. *The Political Economy of Nuclear Energy*; Springer International Publishing: Cham, 2019; ISBN 978-3-030-27028-5.
78. Fleisher, R.L.; Price, P.B.; Walker, R.M. Nuclear Tracks in Solids: Principles and Applications. *Berkeley* **1975**.
79. Fleischer, R.L. Etching Nuclear Tracks. In *Tracks to Innovation*; Springer New York: New York, NY, 1998; pp. 1–25 ISBN 978-1-4612-4452-3.
80. Saifulin, M.M.; O'Connell, J.H.; Janse van Vuuren, A.; Skuratov, V.A.; Kirilkin, N.S.; Zdorovets, M.V. Latent Tracks in Bulk Yttrium-Iron Garnet Crystals Irradiated with Low and High Velocity Krypton and Xenon Ions. *Nucl Instrum Methods Phys Res B* **2019**, *460*, 98–103, doi:10.1016/j.nimb.2018.11.023.
81. Fink, D. *Transport Processes in Ion-Irradiated Polymers*; Springer Series in Materials Science; Springer Berlin Heidelberg: Berlin, Heidelberg, 2004; Vol. 65; ISBN 978-3-642-05894-3.
82. Young, D.A. Etching of Radiation Damage in Lithium Fluoride. *Nature 1958 182:4632* **1958**, *182*, 375–377, doi:10.1038/182375a0.
83. Price, P.B.; Walker, R.M. Chemical Etching of Charged-Particle Tracks in Solids. *J Appl Phys* **1962**, *33*, 3407–3412, doi:10.1063/1.1702421.
84. Zhang, X.; Dai, Y.; Sun, J.; Shen, J.; Lin, M.; Xia, F. Solid-State Nanopore/Nanochannel Sensors with Enhanced Selectivity through Pore-in Modification. *Anal Chem* **2024**, *96*, 2277–2285, doi:10.1021/acs.analchem.3c05228.
85. Zhang, Y.; Kong, X.-Y.; Gao, L.; Tian, Y.; Wen, L.; Jiang, L. Fabrication of Nanochannels. *Materials* **2015**, *8*, 6277–6308, doi:10.3390/ma8095304.
86. Hou, X.; Zhang, H.; Jiang, L. Building Bio-Inspired Artificial Functional Nanochannels: From Symmetric to Asymmetric Modification. *Angewandte Chemie International Edition* **2012**, *51*, 5296–5307, doi:10.1002/anie.201104904.
87. Zhang, Z.; Wen, L.; Jiang, L. Bioinspired Smart Asymmetric Nanochannel Membranes. *Chem Soc Rev* **2018**, *47*, 322–356, doi:10.1039/C7CS00688H.
88. Pérez-Mitta, G.; Peinetti, A.S.; Cortez, M.L.; Toimil-Molares, M.E.; Trautmann, C.; Azzaroni, O. Highly Sensitive Biosensing with Solid-State Nanopores Displaying Enzymatically Reconfigurable Rectification Properties. *Nano Lett* **2018**, *18*, 3303–3310, doi:10.1021/acs.nanolett.8b01281.

© 2025 by the author(s). Distributed under a Creative Commons CC BY license.

Preprints.org (www.preprints.org) | NOT PEER-REVIEWED | Posted: 2 July 2025 doi:10.20944/preprints202507.0128.v1

89. Toum Terrones, Y.; Laucirica, G.; Cayón, V.M.; Fenoy, G.E.; Cortez, M.L.; Toimil-Molares, M.E.; Trautmann, C.; Mamisollé, W.A.; Azzaroni, O. Highly Sensitive Acetylcholine Biosensing via Chemical Amplification of Enzymatic Processes in Nanochannels. *Chemical Communications* **2022**, *58*, 10166–10169, doi:10.1039/D2CC02249D.
90. Peinetti, A.S.; Cortez, M.L.; Toimil-Molares, M.E.; Azzaroni, O. Nanoprecipitation-Enhanced Sensitivity in Enzymatic Nanofluidic Biosensors. *Anal Chem* **2024**, *96*, 5282–5288, doi:10.1021/acs.analchem.4c00203.
91. Parra, L.M.H.; Laucirica, G.; Toimil-Molares, M.E.; Marmisollé, W.; Azzaroni, O. Sensing Creatinine in Urine via the Iontronic Response of Enzymatic Single Solid-State Nanochannels. *Biosens Bioelectron* **2025**, *268*, 116893, doi:10.1016/j.bios.2024.116893.
92. Gramajo, M.E.; Otero Maffoni, L.; Hernández Parra, L.M.; Marmisollé, W.A.; Cortez, M.L.; Toimil-Molares, M.E.; Peinetti, A.S.; Azzaroni, O. Harnessing Concerted Functions in Confined Environments: Cascading Enzymatic Reactions in Nanofluidic Biosensors for Sensitive Detection of Arginine. *Chemical Communications* **2025**, *61*, 697–700, doi:10.1039/D4CC04703F.
93. Apel, P.Y.; Blonskaya, I. V.; Orelovitch, O.L.; Root, D.; Vutsadakis, V.; Dmitriev, S.N. Effect of Nanosized Surfactant Molecules on the Etching of Ion Tracks: New Degrees of Freedom in Design of Pore Shape. *Nucl Instrum Methods Phys Res B* **2003**, *209*, 329–334, doi:10.1016/S0168-583X(02)02057-8.
94. Apel, P.Yu.; Blonskaya, I.V.; Dmitriev, S.N.; Mamonova, T.I.; Orelovitch, O.L.; Sartowska, B.; Yamauchi, Y. Surfactant-Controlled Etching of Ion Track Nanopores and Its Practical Applications in Membrane Technology. *Radiat Meas* **2008**, *43*, S552–S559, doi:10.1016/j.radmeas.2008.04.057.
95. Karim, S.; Ensinger, W.; Mujahid, S.A.; Maaz, K.; Khan, E.U. Effect of Etching Conditions on Pore Shape in Etched Ion-Track Polycarbonate Membranes. *Radiat Meas* **2009**, *44*, 779–782, doi:10.1016/j.radmeas.2009.10.022.
96. Lin, L.; Yan, J.; Li, J. Small-Molecule Triggered Cascade Enzymatic Catalysis in Hour-Glass Shaped Nanochannel Reactor for Glucose Monitoring. *Anal Chem* **2014**, *86*, 10546–10551, doi:10.1021/ac501983a.
97. Gillespie, D.; Boda, D.; He, Y.; Apel, P.; Siwy, Z.S. Synthetic Nanopores as a Test Case for Ion Channel Theories: The Anomalous Mole Fraction Effect without Single Filing. *Biophys J* **2008**, *95*, 609–619, doi:10.1529/biophysj.107.127985.
98. Siwy, Z.S. Ion-Current Rectification in Nanopores and Nanotubes with Broken Symmetry. *Adv Funct Mater* **2006**, *16*, 735–746, doi:10.1002/adfm.200500471.
99. Hou, G.; Zhang, H.; Xie, G.; Xiao, K.; Wen, L.; Li, S.; Tian, Y.; Jiang, L. Ultratrace Detection of Glucose with Enzyme-Functionalized Single Nanochannels. *J Mater Chem A Mater* **2014**, *2*, 19131–19135, doi:10.1039/C4TA05013D.
100. Pérez-Mitta, G.; Marmisolle, W.A.; Burr, L.; Toimil-Molares, M.E.; Trautmann, C.; Azzaroni, O. Proton-Gated Rectification Regimes in Nanofluidic Diodes Switched by Chemical Effectors. *Small* **2018**, *14*, 1703144, doi:10.1002/smll.201703144.
101. Apel, P.Yu.; Blonskaya, I.V.; Orelovitch, O.L.; Dmitriev, S.N. Diode-like Ion-Track Asymmetric Nanopores: Some Alternative Methods of Fabrication. *Nucl Instrum Methods Phys Res B* **2009**, *267*, 1023–1027, doi:10.1016/j.nimb.2009.02.012.
102. Froehlich, K.; Scheuerlein, M.C.; Ali, M.; Nasir, S.; Ensinger, W. Enhancement of Heavy Ion Track-Etching in Polyimide Membranes with Organic Solvents. *Nanotechnology* **2022**, *33*, 045301, doi:10.1088/1361-6528/ac2f5a.
103. Angel L. Huamani; Gregorio Laucirica; María Eugenia Toimil-Molares; Waldemar Marmisollé; Omar Azzaroni; Matías Rafti Expanding the Synergy between MOFs and Solid-State-Nanochannels: Post-Synthetic Modification for the Covalent Anchoring of Urease in Urea Detection (to be submitted).
104. L. Miguel Hernandez Parra; Marcos E. Gramajo; Lautaro Otero Maffoni; Laucirica Gregorio; Ana S. Peinetti; M. Lorena Cortez; M. Eugenia Toimil-Molares; Waldemar, A.M.; Omar Azzaroni Single Nanochannel-Based Iontronic Detection of Adenosine at Nanomolar Concentrations. *Chemistry - A European Journal* **2025**, *Submitted*.
105. Zhu, L.; Gu, D.; Liu, Q. Hydrogen Peroxide Sensing Based on Inner Surfaces Modification of Solid-State Nanopore. *Nanoscale Res Lett* **2017**, *12*, 422, doi:10.1186/s11671-017-2190-x.

© 2025 by the author(s). Distributed under a Creative Commons CC BY license.

Preprints.org (www.preprints.org) | NOT PEER-REVIEWED | Posted: 2 July 2025 doi:10.20944/preprints202507.0128.v1

106. Ali, M.; Ramirez, P.; Tahir, M.N.; Mafe, S.; Siwy, Z.; Neumann, R.; Tremel, W.; Ensinger, W. Biomolecular Conjugation inside Synthetic Polymer Nanopores via Glycoprotein–Lectin Interactions. *Nanoscale* **2011**, *3*, 1894, doi:10.1039/c1nr00003a.
107. Ali, M.; Tahir, M.N.; Siwy, Z.; Neumann, R.; Tremel, W.; Ensinger, W. Hydrogen Peroxide Sensing with Horseradish Peroxidase-Modified Polymer Single Conical Nanochannels. *Anal Chem* **2011**, *83*, 1673–1680, doi:10.1021/ac102795a.
108. Karimi, K.; Fardoost, A.; Mhatre, N.; Rajan, J.; Boisvert, D.; Javanmard, M. A Thorough Review of Emerging Technologies in Micro- and Nanochannel Fabrication: Limitations, Applications, and Comparison. *Micromachines (Basel)* **2024**, *15*, 1274, doi:10.3390/mi15101274.
109. Li, P.; Chen, S.; Dai, H.; Yang, Z.; Chen, Z.; Wang, Y.; Chen, Y.; Peng, W.; Shan, W.; Duan, H. Recent Advances in Focused Ion Beam Nanofabrication for Nanostructures and Devices: Fundamentals and Applications. *Nanoscale* **2021**, *13*, 1529–1565, doi:10.1039/D0NR07539F.
110. Melngailis, J. Focused Ion Beam Technology and Applications. *Journal of Vacuum Science & Technology B: Microelectronics Processing and Phenomena* **1987**, *5*, 469–495, doi:10.1116/1.583937.
111. Kant, K.; Losic, D. *FIB Nanostructures*; Wang, Z.M., Ed.; Lecture Notes in Nanoscale Science and Technology; Springer International Publishing: Cham, 2013; Vol. 20; ISBN 978-3-319-02873-6.
112. Chen, X.; Zhang, L. Review in Manufacturing Methods of Nanochannels of Bio-Nanofluidic Chips. *Sens Actuators B Chem* **2018**, *254*, 648–659, doi:10.1016/j.snb.2017.07.139.
113. Tseng, A.A. Recent Developments in Nanofabrication Using Focused Ion Beams. *Small* **2005**, *1*, 924–939, doi:10.1002/smll.200500113.
114. Lebedev, D.; Malyshev, G.; Ryzhkov, I.; Mozharov, A.; Shugurov, K.; Sharov, V.; Panov, M.; Tumkin, I.; Afonicheva, P.; Evstrapov, A.; et al. Focused Ion Beam Milling Based Formation of Nanochannels in Silicon-Glass Microfluidic Chips for the Study of Ion Transport. *Microfluid Nanofluidics* **2021**, *25*, 51, doi:10.1007/s10404-021-02450-x.
115. Crnković, A.; Srnko, M.; Anderluh, G. Biological Nanopores: Engineering on Demand. *Life* **2021**, *11*, 27, doi:10.3390/life11010027.
116. Liu, M.; Nothling, M.D.; Zhang, S.; Fu, Q.; Qiao, G.G. Thin Film Composite Membranes for Postcombustion Carbon Capture: Polymers and Beyond. *Prog Polym Sci* **2022**, *126*, 101504, doi:10.1016/j.progpolymsci.2022.101504.
117. Heimann, R.B. Silicon Nitride Ceramics: Structure, Synthesis, Properties, and Biomedical Applications. *Materials* **2023**, *16*, 5142, doi:10.3390/ma16145142.
118. Al-Sabagh, A.M.; Yehia, F.Z.; Eshaq, G.; Rabie, A.M.; ElMetwally, A.E. Greener Routes for Recycling of Polyethylene Terephthalate. *Egyptian Journal of Petroleum* **2016**, *25*, 53–64, doi:10.1016/j.ejpe.2015.03.001.
119. Sinha, V.; Patel, M.R.; Patel, J. V. Pet Waste Management by Chemical Recycling: A Review. *J Polym Environ* **2010**, *18*, 8–25, doi:10.1007/s10924-008-0106-7.
120. Stephans, L.E.; Myles, A.; Thomas, R.R. Kinetics of Alkaline Hydrolysis of a Polyimide Surface. *Langmuir* **2000**, *16*, 4706–4710, doi:10.1021/la991105m.
121. Sypabekova, M.; Hagemann, A.; Rho, D.; Kim, S. Review: 3-Aminopropyltriethoxysilane (APTES) Deposition Methods on Oxide Surfaces in Solution and Vapor Phases for Biosensing Applications. *Biosensors (Basel)* **2022**, *13*, 36, doi:10.3390/bios13010036.
122. Lynch, C.I.; Rao, S.; Sansom, M.S.P. Water in Nanopores and Biological Channels: A Molecular Simulation Perspective. *Chem Rev* **2020**, *120*, 10298–10335, doi:10.1021/acs.chemrev.9b00830.
123. Xie, G.; Li, P.; Zhao, Z.; Zhu, Z.; Kong, X.-Y.; Zhang, Z.; Xiao, K.; Wen, L.; Jiang, L. Light- and Electric-Field-Controlled Wetting Behavior in Nanochannels for Regulating Nanoconfined Mass Transport. *J Am Chem Soc* **2018**, *140*, 4552–4559, doi:10.1021/jacs.7b13136.
124. Birkner, J.P.; Poolman, B.; Koçer, A. Hydrophobic Gating of Mechanosensitive Channel of Large Conductance Evidenced by Single-Subunit Resolution. *Proceedings of the National Academy of Sciences* **2012**, *109*, 12944–12949, doi:10.1073/pnas.1205270109.
125. Beckstein, O.; Sansom, M.S.P. Liquid–Vapor Oscillations of Water in Hydrophobic Nanopores. *Proceedings of the National Academy of Sciences* **2003**, *100*, 7063–7068, doi:10.1073/pnas.1136844100.

© 2025 by the author(s). Distributed under a Creative Commons CC BY license.

Preprints.org (www.preprints.org) | NOT PEER-REVIEWED | Posted: 2 July 2025 doi:10.20944/preprints202507.0128.v1

126. Powell, M.R.; Cleary, L.; Davenport, M.; Shea, K.J.; Siwy, Z.S. Electric-Field-Induced Wetting and Dewetting in Single Hydrophobic Nanopores. *Nat Nanotechnol* **2011**, *6*, 798–802, doi:10.1038/nnano.2011.189.
127. Xiao, K.; Zhou, Y.; Kong, X.-Y.; Xie, G.; Li, P.; Zhang, Z.; Wen, L.; Jiang, L. Electrostatic-Charge- and Electric-Field-Induced Smart Gating for Water Transportation. *ACS Nano* **2016**, *10*, 9703–9709, doi:10.1021/acsnano.6b05682.
128. Junk, A.; Riess, F. From an Idea to a Vision: There's Plenty of Room at the Bottom. *Am J Phys* **2006**, *74*, 825–830, doi:10.1119/1.2213634.
129. Gouaux, E.; MacKinnon, R. Principles of Selective Ion Transport in Channels and Pumps. *Science (1979)* **2005**, *310*, 1461–1465, doi:10.1126/science.1113666.
130. Sun, C.; Zhou, R.; Zhao, Z.; Bai, B. Nanoconfined Fluids: What Can We Expect from Them? *J Phys Chem Lett* **2020**, *11*, 4678–4692, doi:10.1021/acs.jpclett.0c00591.
131. Plecis, A.; Schoch, R.B.; Renaud, P. Ionic Transport Phenomena in Nanofluidics: Experimental and Theoretical Study of the Exclusion-Enrichment Effect on a Chip. *Nano Lett* **2005**, *5*, 1147–1155, doi:10.1021/nl050265h.
132. Silies, L.; Andrieu-Brunsen, A. Programming Ionic Pore Accessibility in Zwitterionic Polymer Modified Nanopores. *Langmuir* **2018**, *34*, 807–816, doi:10.1021/acs.langmuir.7b00529.
133. Sadeghi, M.; Saidi, M.H.; Moosavi, A.; Kröger, M. Tuning Electrokinetic Flow, Ionic Conductance, and Selectivity in a Solid-State Nanopore Modified with a PH-Responsive Polyelectrolyte Brush: A Molecular Theory Approach. *The Journal of Physical Chemistry C* **2020**, *124*, 18513–18531, doi:10.1021/acs.jpcc.0c02904.
134. Gilles, F.M.; Tagliazucchi, M.; Azzaroni, O.; Szleifer, I. Ionic Conductance of Polyelectrolyte-Modified Nanochannels: Nanoconfinement Effects on the Coupled Protonation Equilibria of Polyprotic Brushes. *The Journal of Physical Chemistry C* **2016**, *120*, 4789–4798, doi:10.1021/acs.jpcc.5b11788.
135. Tagliazucchi, M.; Azzaroni, O.; Szleifer, I. Responsive Polymers End-Tethered in Solid-State Nanochannels: When Nanoconfinement Really Matters. *J Am Chem Soc* **2010**, *132*, 12404–12411, doi:10.1021/ja104152g.
136. Tagliazucchi, M.; Szleifer, I. Stimuli-Responsive Polymers Grafted to Nanopores and Other Nano-Curved Surfaces: Structure, Chemical Equilibrium and Transport. *Soft Matter* **2012**, *8*, 7292, doi:10.1039/c2sm25777g.
137. Laucirica, G.; Hernández Parra, L.M.; Huamani, A.L.; Wagner, M.F.; Albesa, A.G.; Toimil-Molares, M.E.; Marmisollé, W.; Azzaroni, O. Insight into the Transport of Ions from Salts of Moderated Solubility through Nanochannels: Negative Incremental Resistance Assisted by Geometry. *Nanoscale* **2024**, *16*, 12599–12610, doi:10.1039/D3NR06212K.
138. Kurupath, V.P.; Coasne, B. Mixture Adsorption in Nanoporous Zeolite and at Its External Surface: In-Pore and Surface Selectivity. *J Phys Chem B* **2023**, *127*, 9596–9607, doi:10.1021/acs.jpcb.3c04221.
139. Zhang, X.; Shen, J.; Pan, S.; Qian, J.; Pan, B. Metastable Zirconium Phosphate under Nanoconfinement with Superior Adsorption Capability for Water Treatment. *Adv Funct Mater* **2020**, *30*, 1909014, doi:10.1002/adfm.201909014.
140. Dai, H.; Li, Y.; Fu, Y.; Li, Y. Enzyme Catalysis Induced Polymer Growth in Nanochannels: A New Approach to Regulate Ion Transport and to Study Enzyme Kinetics in Nanospace. *Electroanalysis* **2018**, *30*, 328–335, doi:10.1002/elan.201700703.
141. Wang, C.; Ye, D.-K.; Wang, Y.-Y.; Lu, T.; Xia, X.-H. Insights into the "Free State" Enzyme Reaction Kinetics in Nanoconfinement. *Lab Chip* **2013**, *13*, 1546, doi:10.1039/c3lc41319e.
142. Daiguji, H. Ion Transport in Nanofluidic Channels. *Chem. Soc. Rev.* **2010**, *39*, 901–911, doi:10.1039/B820556F.
143. Emmerich, T.; Ronceray, N.; Agrawal, K.V.; Garaj, S.; Kumar, M.; Noy, A.; Radenovic, A. Nanofluidics. *Nature Reviews Methods Primers* **2024**, *4*, 69, doi:10.1038/s43586-024-00344-0.
144. Tagliazucchi, M.; Szleifer, I. Transport Mechanisms in Nanopores and Nanochannels: Can We Mimic Nature? *Materials Today* **2015**, *18*, 131–142, doi:10.1016/j.mattod.2014.10.020.
145. Schoch, R.B.; Han, J.; Renaud, P. Transport Phenomena in Nanofluidics. *Rev Mod Phys* **2008**, *80*, 839–883, doi:10.1103/RevModPhys.80.839.
146. Nazari, M.; Davoodabadi, A.; Huang, D.; Luo, T.; Ghasemi, H. Transport Phenomena in Nano/Molecular Confinements. *ACS Nano* **2020**, *14*, 16348–16391, doi:10.1021/acsnano.0c07372.

© 2025 by the author(s). Distributed under a Creative Commons CC BY license.

Preprints.org (www.preprints.org) | NOT PEER-REVIEWED | Posted: 2 July 2025 doi:10.20944/preprints202507.0128.v1

147. Shen, J.; Liu, G.; Han, Y.; Jin, W. Artificial Channels for Confined Mass Transport at the Sub-Nanometre Scale. *Nat Rev Mater* **2021**, *6*, 294–312, doi:10.1038/s41578-020-00268-7.
148. Karayannidis, G.P.; Chatziavgoustis, A.P.; Achilias, D.S. Poly(Ethylene Terephthalate) Recycling and Recovery of Pure Terephthalic Acid by Alkaline Hydrolysis. *Advances in Polymer Technology* **2002**, *21*, 250–259, doi:10.1002/adv.10029.
149. Karnik, R.; Fan, R.; Yue, M.; Li, D.; Yang, P.; Majumdar, A. Electrostatic Control of Ions and Molecules in Nanofluidic Transistors. *Nano Lett* **2005**, *5*, 943–948, doi:10.1021/nl050493b.
150. Wang, M.; Revil, A. Electrochemical Charge of Silica Surfaces at High Ionic Strength in Narrow Channels. *J Colloid Interface Sci* **2010**, *343*, 381–386, doi:10.1016/j.jcis.2009.11.039.
151. Stein, D.; Kruithof, M.; Dekker, C. Surface-Charge-Governed Ion Transport in Nanofluidic Channels. *Phys Rev Lett* **2004**, *93*, 035901, doi:10.1103/PhysRevLett.93.035901.
152. Brown, M.A.; Abbas, Z.; Kleibert, A.; Green, R.G.; Goel, A.; May, S.; Squires, T.M. Determination of Surface Potential and Electrical Double-Layer Structure at the Aqueous Electrolyte-Nanoparticle Interface. *Phys Rev X* **2016**, *6*, 011007, doi:10.1103/PhysRevX.6.011007.
153. Doblhoff-Dier, K.; Koper, M.T.M. Modeling the Gouy–Chapman Diffuse Capacitance with Attractive Ion–Surface Interaction. *The Journal of Physical Chemistry C* **2021**, *125*, 16664–16673, doi:10.1021/acs.jpcc.1c02381.
154. Martinsen, Ø.G.; Heiskanen, A. *Bioimpedance and Bioelectricity Basics*; Elsevier, 2023; ISBN 9780128191071.
155. Stojek, Z. The Electrical Double Layer and Its Structure. In *Electroanalytical Methods*; Springer Berlin Heidelberg: Berlin, Heidelberg, 2010; pp. 3–9 ISBN 978-3-642-02915-8.
156. Saboorian-Jooybari, H.; Chen, Z. Calculation of Re-Defined Electrical Double Layer Thickness in Symmetrical Electrolyte Solutions. *Results Phys* **2019**, *15*, 102501, doi:10.1016/j.rinp.2019.102501.
157. Hunter, R.J..; Ottewill, R.H..; Rowell, R.L.. Zeta Potential in Colloid Science : Principles and Applications. **2014**, 399.
158. Zhou, K.; Perry, J.M.; Jacobson, S.C. Transport and Sensing in Nanofluidic Devices. *Annual Review of Analytical Chemistry* **2011**, *4*, 321–341, doi:10.1146/annurev-anchem-061010-113938.
159. Zhong, J.; Alibakhshi, M.A.; Xie, Q.; Riordon, J.; Xu, Y.; Duan, C.; Sinton, D. Exploring Anomalous Fluid Behavior at the Nanoscale: Direct Visualization and Quantification via Nanofluidic Devices. *Acc Chem Res* **2020**, *53*, 347–357, doi:10.1021/acs.accounts.9b00411.
160. Sparreboom, W.; van den Berg, A.; Eijkel, J.C.T. Principles and Applications of Nanofluidic Transport. *Nat Nanotechnol* **2009**, *4*, 713–720, doi:10.1038/nnano.2009.332.
161. Haywood, D.G.; Harms, Z.D.; Jacobson, S.C. Electroosmotic Flow in Nanofluidic Channels. *Anal Chem* **2014**, *86*, 11174–11180, doi:10.1021/ac502596m.
162. Qiao, N.; Zhang, Z.; Liu, Z.; Lu, W.; Li, C. Ion Current Rectification in Asymmetric Nanochannels: Effects of Nanochannel Shape and Surface Charge. *Int J Heat Mass Transf* **2023**, *208*, 124038, doi:10.1016/j.ijheatmasstransfer.2023.124038.
163. Laucirica, G.; Albesa, A.G.; Toimil-Molares, M.E.; Trautmann, C.; Marmisollé, W.A.; Azzaroni, O. Shape Matters: Enhanced Osmotic Energy Harvesting in Bullet-Shaped Nanochannels. *Nano Energy* **2020**, *71*, 104612, doi:10.1016/j.nanoen.2020.104612.
164. Karimzadeh, M.; Seifollahi, Z.; Khatibi, M.; Ashrafizadeh, S.N. Impacts of the Shape of Soft Nanochannels on Their Ion Selectivity and Current Rectification. *Electrochim Acta* **2021**, *399*, 139376, doi:10.1016/j.electacta.2021.139376.
165. Ghosal, S.; Sherwood, J.D.; Chang, H.-C. Solid-State Nanopore Hydrodynamics and Transport. *Biomicrofluidics* **2019**, *13*, 11301, doi:10.1063/1.5083913.
166. Hou, X.; Guo, W.; Jiang, L. Biomimetic Smart Nanopores and Nanochannels. *Chem Soc Rev* **2011**, *40*, 2385, doi:10.1039/c0cs00053a.
167. Kubeil, C.; Bund, A. The Role of Nanopore Geometry for the Rectification of Ionic Currents. *The Journal of Physical Chemistry C* **2011**, *115*, 7866–7873, doi:10.1021/jp111377h.
168. Cervera, J.; Schiedt, B.; Neumann, R.; Mafé, S.; Ramírez, P. Ionic Conduction, Rectification, and Selectivity in Single Conical Nanopores. *J Chem Phys* **2006**, *124*, doi:10.1063/1.2179797.

© 2025 by the author(s). Distributed under a Creative Commons CC BY license.

Preprints.org (www.preprints.org) | NOT PEER-REVIEWED | Posted: 2 July 2025 doi:10.20944/preprints202507.0128.v1

169. Ramírez, P.; Apel, P.Y.; Cervera, J.; Mafé, S. Pore Structure and Function of Synthetic Nanopores with Fixed Charges: Tip Shape and Rectification Properties. *Nanotechnology* **2008**, *19*, 315707, doi:10.1088/0957-4484/19/31/315707.
170. Guo, W.; Tian, Y.; Jiang, L. Asymmetric Ion Transport through Ion-Channel-Mimetic Solid-State Nanopores. *Acc Chem Res* **2013**, *46*, 2834–2846, doi:10.1021/ar400024p.
171. Chuang, P.Y.; Hsu, J.P. Influence of Shape and Charged Conditions of Nanopores on Their Ionic Current Rectification, Electroosmotic Flow, and Selectivity. *Colloids Surf A Physicochem Eng Asp* **2023**, *658*, 130696, doi:10.1016/J.COLSURFA.2022.130696.
172. Xiao, K.; Wen, L.; Jiang, L. Biomimetic Solid-State Nanochannels: From Fundamental Research to Practical Applications. *Small* **2016**, *12*, 2810–2831, doi:10.1002/smll.201600359.
173. White, H.S.; Bund, A. Ion Current Rectification at Nanopores in Glass Membranes. *Langmuir* **2008**, *24*, 2212–2218, doi:10.1021/la702955k.
174. Vlassiouk, I.; Smirnov, S.; Siwy, Z. Ionic Selectivity of Single Nanochannels. *Nano Lett* **2008**, *8*, 1978–1985, doi:10.1021/nl800949k.
175. Yameen, B.; Ali, M.; Neumann, R.; Ensinger, W.; Knoll, W.; Azzaroni, O. Ionic Transport Through Single Solid-State Nanopores Controlled with Thermally Nanoactuated Macromolecular Gates. *Small* **2009**, *5*, 1287–1291, doi:10.1002/smll.200801318.
176. Punekar, N.S. *ENZYMES: Catalysis, Kinetics and Mechanisms*; Springer Nature Singapore: Singapore, 2025; ISBN 978-981-97-8178-2.
177. Berg, J.M.; Gatto, G.J.; Hines, J.K.; Tymoczko, J.L. *Biochemistry (-2024)*; Macmillan Learning, 2024; ISBN 1319417469.
178. Gao, Y.; Kyratzis, I. Covalent Immobilization of Proteins on Carbon Nanotubes Using the Cross-Linker 1-Ethyl-3-(3-Dimethylaminopropyl)Carbodiimide—a Critical Assessment. *Bioconjug Chem* **2008**, *19*, 1945–1950, doi:10.1021/bc800051c.
179. Arafat, A.; Giesbers, M.; Rosso, M.; Sudhölter, E.J.R.; Schroën, K.; White, R.G.; Yang, L.; Linford, M.R.; Zuilhof, H. Covalent Biofunctionalization of Silicon Nitride Surfaces. *Langmuir* **2007**, *23*, 6233–6244, doi:10.1021/la7007045.
180. Guisan, J.M.; Fernandez-Lorente, G.; Rocha-Martin, J.; Moreno-Gamero, D. Enzyme Immobilization Strategies for the Design of Robust and Efficient Biocatalysts. *Curr Opin Green Sustain Chem* **2022**, *35*, 100593, doi:10.1016/j.cogsc.2022.100593.
181. Liu, T.; Yin, Y.; Yang, Y.; Russell, T.P.; Shi, S. Layer-by-Layer Engineered All-Liquid Microfluidic Chips for Enzyme Immobilization. *Advanced Materials* **2022**, *34*, 2105386, doi:10.1002/adma.202105386.
182. Ariga, K.; Ji, Q.; Hill, J.P. Enzyme-Encapsulated Layer-by-Layer Assemblies: Current Status and Challenges Toward Ultimate Nanodevices. In; Springer, Berlin, Heidelberg, 2010; pp. 51–87 ISBN 978-3-642-12873-8.
183. Argaman, O.; Ben-Barak Zelas, Z.; Fishman, A.; Rytwo, G.; Radian, A. Immobilization of Aldehyde Dehydrogenase on Montmorillonite Using Polyethyleneimine as a Stabilization and Bridging Agent. *Appl Clay Sci* **2021**, *212*, 106216, doi:10.1016/j.clay.2021.106216.
184. Mantione, D.; del Agua, I.; Schaafsma, W.; ElMahmoudy, M.; Uguz, I.; Sanchez-Sanchez, A.; Sardon, H.; Castro, B.; Malliaras, G.G.; Mecerreyes, D. Low-Temperature Cross-Linking of PEDOT:PSS Films Using Divinylsulfone. *ACS Appl Mater Interfaces* **2017**, *9*, 18254–18262, doi:10.1021/acsami.7b02296.
185. Morales-Sanfrutos, J.; Lopez-Jaramillo, F.; Elremaily, M.; Hernández-Mateo, F.; Santoyo-Gonzalez, F. Divinyl Sulfone Cross-Linked Cyclodextrin-Based Polymeric Materials: Synthesis and Applications as Sorbents and Encapsulating Agents. *Molecules* **2015**, *20*, 3565–3581, doi:10.3390/molecules20033565.
186. Ruckenstein, E.; Rajora, P. Optimization of the Activity in Porous Media of Proton-generating Immobilized Enzymatic Reactions by Weak Acid Facilitation. *Biotechnol Bioeng* **1985**, *27*, 807–817, doi:10.1002/bit.260270609.
187. Li, J.; An, P.; Qin, C.; Sun, C.-L.; Sun, M.; Ji, Z.; Wang, C.; Du, G.; Liu, J.; Xie, Y. Bioinspired Dual-Responsive Nanofluidic Diodes by Poly-L-Lysine Modification. *ACS Omega* **2020**, *5*, 4501–4506, doi:10.1021/acsomega.9b03850.
188. Ding, M.; Hou, L.; Duan, X.; Shi, T.; Li, W.; Shi, A.-C. Translocation of Micelles through a Nanochannel. *Macromolecules* **2022**, *55*, 6487–6492, doi:10.1021/acs.macromol.2c00447.

© 2025 by the author(s). Distributed under a Creative Commons CC BY license.

Preprints.org (www.preprints.org) | NOT PEER-REVIEWED | Posted: 2 July 2025 doi:10.20944/preprints202507.0128.v1

189. Zhu, Z.; Wang, D.; Tian, Y.; Jiang, L. Ion/Molecule Transportation in Nanopores and Nanochannels: From Critical Principles to Diverse Functions. *J Am Chem Soc* **2019**, *141*, 8658–8669, doi:10.1021/jacs.9b00086.
190. Perez Sirkin, Y.A.; Vigil De Maio, M.; Tagliazucchi, M. Mechanisms of Enzymatic Transduction in Nanochannel Biosensors. *Chem Asian J* **2022**, *17*, e202200588, doi:10.1002/asia.202200588.
191. Vilozny, B.; Actis, P.; Seger, R.A.; Pourmand, N. Dynamic Control of Nanoprecipitation in a Nanopipette. *ACS Nano* **2011**, *5*, 3191–3197, doi:10.1021/nn200320b.
192. Montero-Jimenez, M.; Lugli-Arroyo, J.; Fenoy, G.E.; Piccinini, E.; Knoll, W.; Marmisollé, W.A.; Azzaroni, O. Transduction of Amine–Phosphate Supramolecular Interactions and Biosensing of Acetylcholine through PEDOT-Polyamine Organic Electrochemical Transistors. *ACS Appl Mater Interfaces* **2024**, *16*, 61419–61427, doi:10.1021/acsami.3c09286.
193. Laucirica, G.; Marmisollé, W.A.; Azzaroni, O. Dangerous Liaisons: Anion-Induced Protonation in Phosphate–Polyamine Interactions and Their Implications for the Charge States of Biologically Relevant Surfaces. *Physical Chemistry Chemical Physics* **2017**, *19*, 8612–8620, doi:10.1039/C6CP08793K.
194. Laucirica, G.; Pérez-Mitta, G.; Toimil-Molares, M.E.; Trautmann, C.; Marmisollé, W.A.; Azzaroni, O. Amine-Phosphate Specific Interactions within Nanochannels: Binding Behavior and Nanoconfinement Effects. *The Journal of Physical Chemistry C* **2019**, *123*, 28997–29007, doi:10.1021/acs.jpcc.9b07977.

Disclaimer/Publisher's Note: The statements, opinions and data contained in all publications are solely those of the individual author(s) and contributor(s) and not of MDPI and/or the editor(s). MDPI and/or the editor(s) disclaim responsibility for any injury to people or property resulting from any ideas, methods, instructions or products referred to in the content.

© 2025 by the author(s). Distributed under a Creative Commons CC BY license.